# A new role for excitation in the retinal direction-selective circuit

Lea Ankri ⬥, Serena Riccitelli ⬥ and Michal Rivlin-Etzion ⬥

Department of Brain Sciences, Weizmann Institute of Science, Rehovot, Israel

Handling Editors: Katalin Toth & Karin Dedek

The peer review history is available in the Supporting Information section of this article (https://doi.org/10.1113/JP286581#support-information-section).
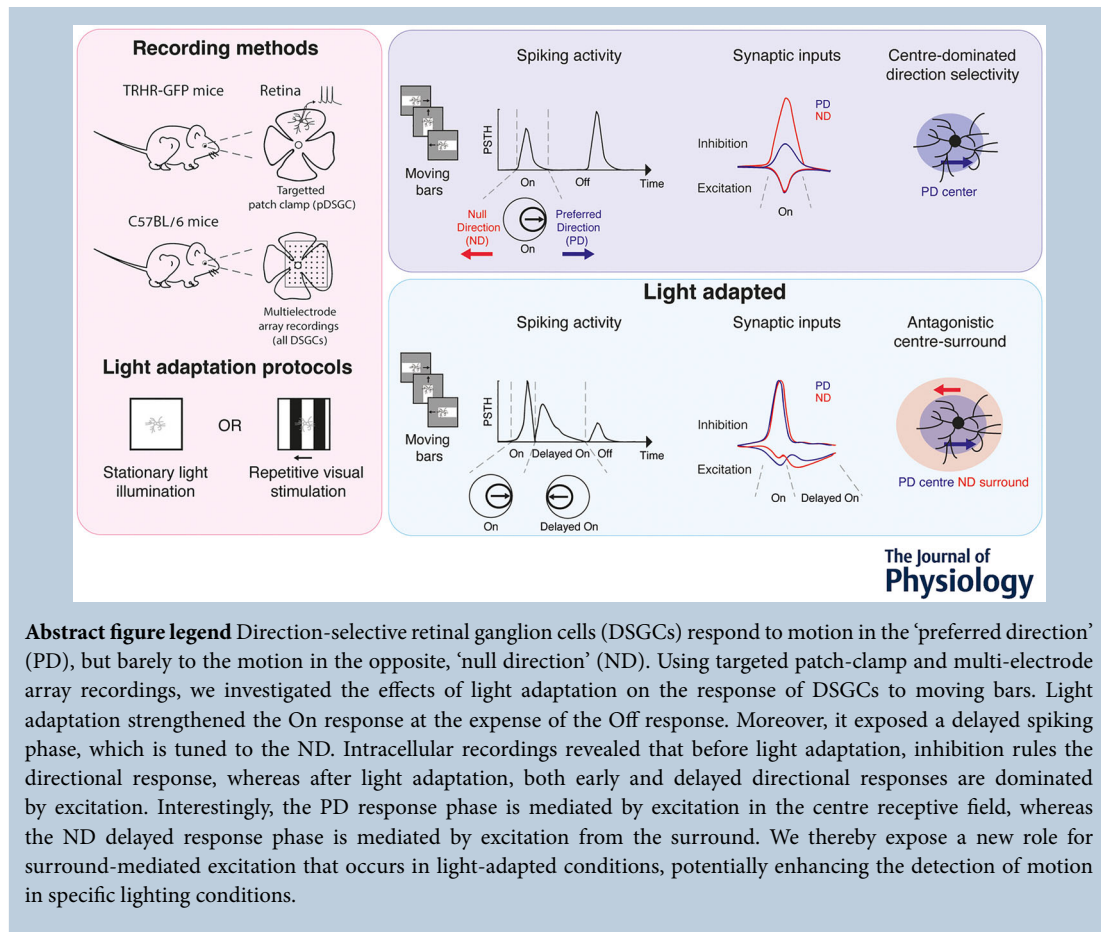
Abstract figure legend Direction-selective retinal ganglion cells (DSGCs) respond to motion in the 'preferred direction' (PD), but barely to the motion in the opposite, 'null direction' (ND). Using targeted patch-clamp and multi-electrode array recordings, we investigated the effects of light adaptation on the response of DSGCs to moving bars. Light adaptation strengthened the On response at the expense of the Off response. Moreover, it exposed a delayed spiking phase, which is tuned to the ND. Intracellular recordings revealed that before light adaptation, inhibition rules the directional response, whereas after light adaptation, both early and delayed directional responses are dominated by excitation. Interestingly, the PD response phase is mediated by excitation in the centre receptive field, whereas the ND delayed response phase is mediated by excitation from the surround. We thereby expose a new role for surround-mediated excitation that occurs in light-adapted conditions, potentially enhancing the detection of motion in specific lighting conditions.

Lea Ankri obtained her PhD in the Rivlin laboratory at the Weizmann Institute of Science and is now a postdoctoral fellow. Her main interest resides in understanding the fundamental laws that underlie neuronal computations in brain circuits. She is intrigued specifically by the retina, from which one can gain profound insights into how general computational motifs manifest in a relatively compact network.
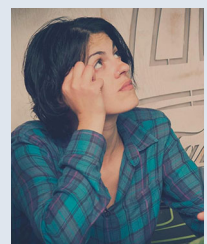
Abstract A key feature of the receptive field of neurons in the visual system is their centre–surround antagonism, whereby the centre and the surround exhibit responses of opposite polarity. This organization is thought to enhance visual acuity, but whether and how such antagonism plays a role in more complex processing remains poorly understood. Here, we investigate the role of centre and surround receptive fields in retinal direction selectivity by exposing posterior-preferring On–Off direction-selective ganglion cells (pDSGCs) to adaptive light and recording their response to globally moving objects. We reveal that light adaptation leads to surround expansion in pDSGCs. The pDSGCs maintain their original directional tuning in the centre receptive field, but present the oppositely tuned response in their surround. Notably, although inhibition is the main substrate for retinal direction selectivity, we found that following light adaptation, both the centre- and surround-mediated responses originate from directionally tuned excitatory inputs. Multi-electrode array recordings show similar oppositely tuned responses in other DSGC subtypes. Together, these data attribute a new role for excitation in the direction-selective circuit. This excitation carries an antagonistic centre–surround property, possibly designed to sharpen the detection of motion direction in the retina.

Corresponding authors L. Ankri and M. Rivlin-Etzion: Department of Brain Sciences, Weizmann Institute of Science, Herzel st. 234, 761000, Rehovot, Israel.   Email: lea.ankri@weizmann.ac.il and michal.rivlin@weizmann.ac.il

Key points

- Receptive fields of direction-selective retinal ganglion cells expand asymmetrically following light adaptation.
- The increase in the surround receptive field generates a delayed spiking phase that is tuned to the null direction and is mediated by excitation.
- Following light adaptation, excitation rules the computation in the centre receptive field and is tuned to the preferred direction.
- GABAergic and glycinergic inputs modulate the null-tuned delayed response differentially.
- Null-tuned delayed spiking phases can be detected in all types of direction-selective retinal ganglion cells.
- Light adaptation exposes a hidden directional excitation in the circuit, which is tuned to opposite directions in the centre and surround receptive fields.

Introduction

The visual system encounters a wide range of intensities in everyday visual scenes, requiring the neural code of the retina to adjust to the environment dynamically. To mitigate this problem, the retina uses several adaptational mechanisms that enable accommodation over different temporal and spatial scales (Demb, 2008; Rieke & Rudd, 2009; Rivlin-Etzion et al., 2018). One example of such accommodation is the centre–surround reorganization of retinal cells. Retinal ganglion cells display opposite polarity preferences in their centre and surround receptive fields (On-centre–Off-surround or vice versa). This organization is a hallmark of visual neurons and is thought to sharpen visual acuity (Derrington & Lennie, 1982; Marr & Hildreth, 1980). Yet, the relative contribution of the centre and surround of retinal cells is flexible and can change in different lighting conditions (Barlow et al., 1957; Cowan et al., 2017; Dedek et al., 2008; Kuffler, 1953; Nath et al., 2023). Light adaptational processes are investigated using different protocols that can have distinct outcomes. One approach uses a stepwise increase in light intensity, whereby the light level is raised systematically in increments (Farrow et al., 2013; Nath et al., 2023; Pearson & Kerschensteiner, 2015; Tikidji-Hamburyan et al., 2015; Yao et al., 2018). Another approach uses steady or pulsed light stimulations, whereby the neuronal response is tested before and after exposing the retina to intensive light for a given period of time (Cicerone et al., 1979; Enroth-Cugell & Pinto, 1972; Rivlin-Etzion et al., 2012; Sagdullaev & McCall, 2005; Vlasits et al., 2014). Despite the diversity of protocols,

changes in centre–surround antagonism of retinal cells are widely reported, with strengthening of the antagonistic surround following light adaptation (Ankri et al., 2020; Farrow et al., 2013; Nath et al., 2023; Pearson & Kerschensteiner, 2015; Sagdullaev & McCall, 2005; Yao et al., 2018). Such surround strengthening can either reduce a central response via surround inhibition or elicit a response of opposite polarity, referred to as surround activation (Chaffiol et al., 2017; Fahey & Burkhardt, 2003; Kuffler, 1953; Warwick et al., 2023; Wienbar & Schwartz, 2018).

Although centre–surround reorganization was investigated thoroughly through the prism of polarity shifts, whether it alters the fundamental visual feature encoded by each retinal cell type is still being debated (Wienbar & Schwartz, 2018). One such feature is retinal direction selectivity. In the classical view, the directional response in direction-selective ganglion cells (DSGCs) is determined by asymmetric inhibition from starburst amacrine cells (SACs), which is stronger and faster in response to motion in the null direction, i.e. the direction opposite to the preferred direction of the DSGCs (Ankri et al., 2020; Briggman et al., 2011; Fried et al., 2002; Fried et al., 2005; Pei et al., 2015; Taylor & Vaney, 2002). Our previous study showing that a shift in the timing of SAC inhibition might reverse the directional preference of DSGCs to a drifting grating (Ankri et al., 2020) further emphasizes the role of inhibition. However, the role of excitation in direction selectivity remains controversial, although several lines of evidence support its contribution to the computation (Hanson et al., 2019; Matsumoto et al., 2021; Poleg-Polsky & Diamond, 2016a,b; Sethuramanujam et al., 2016; Strauss et al., 2022; Trenholm et al., 2011).

Here, we resolve the contribution of the centre–surround organization to the computation of motion direction by exposing the cells to different forms of light stimulation. We recorded from On–Off posterior-preferring DSGCs (pDSGCs) while presenting them with globally moving objects that activate their entire receptive field sequentially. We show that before light adaptation, the receptive fields are small and localized, but after exposure to adaptive light, the receptive fields expand owing to enhancement of the surround. This adaptation-mediated alteration in receptive field organization uncovered directional excitation to pDSGCs that is tuned to the preferred direction of the cell in the centre and to the null direction in the surround. Our results demonstrate how flexibility in centre–surround receptive field organization is manifested in the computation of motion direction.

Methods

Animals

Two-photon targeted recordings from DSGCs were performed using Drd4-EGFP (http://www.mmrrc.org/strains/231/0231.html) and Trhr-EGFP (http://www.mmrrc.org/strains/30036/030036.html) mice that express green fluorescent protein (GFP) in posterior-preferring On–Off DSGCs (pDSGCs) (Huberman et al., 2009; Rivlin-Etzion et al., 2011). For multi-electrode array (MEA) recordings, C57BL/6JOlaHsd wild-type mice were used. Mice were 4–12 weeks old and of either sex. Mice had free access to water and food. All procedures were approved by the Institutional Animal Care and Use Committee at the Weizmann Institute of Science.

Electrophysiological recordings

Mice were dark adapted for ≥30 min before anaesthesia in a 300 ml glass chamber containing 1–2 ml isoflurane, followed by decapitation. The retina was extracted and dissected in oxygenated Ames medium (Sigma, St. Louis, MO, USA) under dim red and infrared light. The isolated retina (dorsal part) was then mounted on a 0.22 mm membrane filter (Millipore), with a pre-cut window to allow light to reach the retina, and placed under a two-photon microscope (Bruker, Billerica, MA, USA) equipped with a Mai-Tai laser (Spectra-physics, Santa Clara, CA, USA), as previously described (Warwick et al., 2018). The GFP cells were targeted for recordings with the laser set to 920 nm, to activate photoreceptors minimally, and using a ×60 water-immersion objective (Olympus, Tokyo, Japan). The isolated retina was perfused with warm Ames solution (32–34°C) and equilibrated with carbogen (95% O_2–5% CO_2), and its orientation was maintained (Wei et al., 2011).

Spike recordings from DSGCs were made in loose-patch mode using 4–7 MΩ glass pipettes filled with Ames solution. Voltage-clamp whole-cell recordings from DSGCs were made using 5–9 MΩ glass electrodes filled with intracellular solution containing (mM): 110 CsMeSO₃, 2.8 NaCl, 4 EGTA, 20 Hepes, 5 TEA-Cl, 4 Mg-ATP, 0.3 Na₃GTP and 10 Na₂-phosphocreatine; in some cases, 0.025 AlexaFluor 594 was included (pH adjusted to 7.2 with CsOH; osmolarity = 290 mOsm; $E_{Cl} = -73$ mV). The holding voltages for measuring excitation and inhibition after correction for the liquid junction potential were 0 and −60 mV, respectively. A portion of the cells were recorded in both conditions, i.e. before and after stationary light adaptation, or before and after repetitive visual stimulation (RVS), and a portion

of the cells was recorded in one condition only. This ensured that the effects of light adaptation were not attributable to prolonged intracellular recordings. Data were acquired using pCLAMP10, filtered at 2 kHz and digitized at 10 kHz with a MultiClamp 700B amplifier (Molecular Devices, CA, USA) and a Digidata 1550 digitizer (Molecular Devices).

For pharmacological manipulations, SR95531 (50 μM; Sigma) was used to block GABA$_A$ receptors, strychnine (1 μM; Sigma) to block glycine receptors and L-2-amino-4-phosphonobutyric acid (L-AP4, 20 μM; Sigma) to block On pathway inputs. The drugs were mixed with the bath Ames medium.

Multi-electrode array recordings

Retinal tissue was isolated as described above. Next, the tissue was placed on a multi-electrode array (MEA) pre-coated with a poly-D-lysine solution (PDL, 1.0 mg/ml in H$_2$O; Merck-Millipore, catalogue no. A-003-E) for 1 h at room temperature, with the retinal ganglion cell layer facing the electrodes. All procedures were performed in dim red and infrared light, and the room was dark throughout the experiment.

The MEA recordings were performed using MEAs of 252 electrodes (MultiChannel Systems, 100 or 200 μm minimal electrode distance) while projecting light stimuli focused on the photoreceptor layer, as previously described (Warwick et al., 2024, 2023). Briefly, the retina was perfused with an oxygenated bicarbonate-buffered Ames medium at a flow rate of 3.5 ml/min, and the temperature was maintained at 33.2°C. Data acquisition started 1 h after the retina was placed in the chamber, to allow the spike amplitude to stabilize. Extracellular voltage signals were amplified, digitized at 20 kHz, and saved for offline analysis. Spike sorting and subsequent manual curation were performed using Kilosort2.0 (Pachitariu et al., 2016) and Phy (Rossant & Harris, 2013; Rossant et al., 2016). Only well-separated units were included in the analysis, as determined by refractory period violations <1% (Segev et al., 2004).

Light stimuli

Visual stimuli for patch-clamp recordings were generated using Psychophysics Toolbox in Matlab and projected to the retina by a monochromatic organic light-emitting display (OLED-XL, 800 × 600 pixels, 85 Hz refresh rate; eMagin, Bellevue, WA, USA), through either a ×60 or ×20 objective (UMPLFLN60xW/UMPLFLN20xW; Olympus, Tokyo, Japan). All experiments were carried out in the photopic light range, with the bright light intensity ranging between 1.3×10^4 rod isomerizations (R*/rod/s) for stimuli projected through the ×60 objective and

5.2×10^3 R*/rod/s for the ×20 objective. Visual stimuli were centred on the soma of the recorded cell and focused on the photoreceptor layer.

Directional responses of DSGCs were assessed from the responses to drifting gratings (900 μm/s, 2 Hz, 450 μm/cycle) in 12 different directions, projected via the ×60 objective for 3 s and repeated four times in a pseudo-random order. Full-field gratings were projected via a ×20 objective, while speed, temporal frequency and spatial frequency were adjusted accordingly. The RVS consisted of drifting gratings (900 μm/s, 2 Hz, 450 μm/cycle) moving in the preferred and null directions for 40 s and repeated up to four times (∼5.5 minutes maximum). Stationary light adaptation was simply a white full-field presentation delivered through the ×60 objective for the same time course as RVS.

The bars moved in 12 different directions with a velocity of 900 μm/s; they had a width of 300 μm and length of 1200 μm; and they were projected via the ×20 objective and repeated four times in a pseudo-random order (in the raster plots throughout the manuscript, the traces were reordered for presentation purposes). The bars covered an overall area of 1 mm. For velocity tuning experiments, bars had the same parameters but three different velocities: 450, 900 and 1800 μm/s.

To measure their receptive field, DSGCs were presented with static spots along their preferred–null axis, with a 50 μm white spot on a black background centred on the soma of the cell. Each consecutive spot centre was located 100 μm away from the previous one (centre to centre), and its radius was 30% larger than the neighbouring spot (i.e. proximal to the soma). Each spot was presented for 1 s and repeated two times. Sensitization of pDSGCs was measured by the presentation of a bright spot on a dark background, centred on the soma (50 μm radius; 10 repetitions) for 2 s.

Visual stimuli for MEA recordings were projected via a monochromatic white OLED display (eMagin, EMA-100309-01 SVGA+, 600 × 800 square pixels, 60 Hz refresh rate) through a telecentric lens (Edmund Optics, 2.0X, #58-431) onto the photoreceptors. The pixel size on the retina was 7.5 μm. At maximal brightness, the irradiance used in the experiments was 2.43×10^3 R*/rod/s, whereas the minimum brightness was 7.04 R*/rod/s. Prior to the presentation of moving bars, the retina was presented with 9.44 ± 11.6 min of different stimuli (full-field spot stimulus and gratings). In some of the experiments, a white-noise stimulus was also presented. To determine the polarity preference of cells, we flashed a full-field spot stimulus (radius 1125 μm) consisting of 3 s light offset, 2 s light onset and 3 s light offset. To identify direction-selective cells, we presented square-wave gratings of 100% contrast and a spatial frequency of 397.5 μm that moved in eight equidistant directions in a pseudo-random order at a speed of 795

µm/s (2 Hz). The moving bar stimulus consisted of a white bar on a black background or a black bar on a grey background (900 µm width × 2500–3750 µm length) that moved in eight different pseudo-random directions, at 45° intervals, at a speed of 600 µm/s. To calculate the receptive field of the cells, we applied a white-noise stimulus consisting of black-and-white squares, 60 µm^2 in size, changing at 30 Hz for 15 min, at the end of presentation of all visual stimuli. Each trial was preceded by a 500 ms period of the stimulus background. The long axis of the bar was parallel to the direction of movement. All stimuli (except for the white noise) were repeated five times.

Quantification and statistical analysis

Directional tunings and response parameters of DSGCs. For pDSGC patch-clamp recordings, we extracted spike times from the data after offline filtration using a four-pole Butterworth bandpass filter between 80 and 2000 Hz. The original preferred direction of each cell was determined by initially normalizing the average spike count in each direction by the total number of spikes for all directions. The vectorial summation of these normalized responses yielded a vector whose direction was the preferred direction of the cell and whose magnitude was used to estimate the tuning sharpness (normalized vector sum, range between zero and one). The direction-selective index (DSI) for both the DSGC spiking activity and current recordings was calculated as:

$$\text{DSI} = \frac{\text{PD}_R - \text{ND}_R}{\text{PD}_R + \text{ND}_R}, \qquad (1)$$

where PD$_R$ is the average number of spikes (for DSGC spiking) or the amplitude of the response (for pDSGC currents), in the direction closest to the preferred direction; and ND$_R$ is the average number of spikes (or response amplitude) in response to the opposite (null) motion direction. The preferred direction was set according to the first recorded cell within the same retinal piece, prior to any light adaptation protocol, which corresponded to the posterior direction of the preparation (assuming all GFP-positive cells were tuned to the same posterior direction; Huberman et al., 2009; Rivlin-Etzion et al., 2011).

In MEA recordings, we identified DSGCs by analysing the response to moving gratings. We calculated the normalized vector sum and DSI as described above. To examine the calculated direction selectivity using statistical methods, we performed a shuffling test by random shuffling among 40 trials. To test whether the shuffled normalized vector sum was higher than the original normalized vector sum, we performed the bootstrapping method (1000 replications, $P \leq 0.05$). Cells were defined as direction selective if their DSI in response to gratings was >0.3 and their normalized vector sum was >0.15.

Voltage-clamp raw traces are presented after processing with a Savitzky–Golay filter (third degree polynomial; window length: 81). Only cells with an excitation of >40 pA or an inhibition of >70 pA were included in the analysis.

In the MEA recordings, polarity preference was assessed by the On–Off index (OOI):

$$\text{OOI} = \frac{\text{On}_{\text{phase}} - \text{Off}_{\text{phase}}}{\text{On}_{\text{phase}} + \text{Off}_{\text{phase}}}, \qquad (2)$$

where On$_{\text{phase}}$ and Off$_{\text{phase}}$ are the number of spikes during the light onset and light offset periods, respectively. Cells were defined as On if their OOI > 0.6; On–Off if their −0.6 ≤ OOI ≤ 0.6; and Off if their OOI < 0.6.

The On/Off ratio, for the loose-patch recordings, was calculated by dividing the total number of spikes during the On phase by the number of spikes during the Off phase. In Fig. 2*D*, one cell in the stationary light condition was removed from the analysis because it displayed no spikes during the Off phase, and in Fig. 2*E* four cells in the RVS condition were removed from the analysis because they displayed no spikes during the Off phase. The duration of the response to static spots was defined as the time window during the On phase (within the 1 s presentation of spots) when the spiking activity was >2 SD from baseline.

Estimation and characterization of the receptive field of pDSGCs. To assess the receptive field of pDSGCs using static spot stimulation, the responses to each spot were summed according to spot location and size. The baseline activity was subtracted from the responses to the single spots, and a Gaussian filter was applied to the image (50 points average). On and Off receptive fields were assessed from the 0.5 s response upon spot appearance and disappearance, respectively. Note that 3 pDSGCs before light adaptation did not respond to the static spot stimulation and were therefore omitted from this analysis.

To assess the motion receptive field, responses of DSGCs to moving bars were aligned to the location of the bar when the leading edge of the bar entered the dendritic arbor of DSGCs (On motion receptive field). The baseline activity was subtracted from the response. Alignment of the spike times to these bar locations resulted in an array of 800 ms × 800 ms, where each spike is represented by one point on the time axis and 200 points on the *y*-axis, in correspondence to the width of the bar. The resulting array was rescaled to micrometres according to

the velocity of the bar (800 ms = 720 μm), then filtered using a Gaussian filter (50 points average). To calculate the receptive fields according to the current waveforms, the inputs were initially normalized, then aligned to the location of the bars.

The diameter of the receptive field in response to both static spots and moving bars was calculated by summing the averaged response along the preferred–null axis. The diameter included all regions where the stimulus elicited a response. For assessing activity in the surround, we defined the surround as >150 μm from the soma.

Asymmetry index (AI) was calculated by the equation:

$$\mathrm{AI} = \sum_{n=1}^{n=\#\mathrm{radii}} \left(\frac{R_{\mathrm{PS}}(n) - R_{\mathrm{NS}}(n)}{R_{\mathrm{PS}}(n) + R_{\mathrm{NS}}(n)} \right) \times k(n) , \qquad (3)$$

where $R_{\mathrm{PS}}(n)$ and $R_{\mathrm{NS}}(n)$ are the average responses to spots in the preferred and null side, respectively, in the nth radius. The constant $k(n)$ was set for each pair of spots (the preferred side and null side spots that are at the same absolute distance from the centre), weighting the difference in the responses according to the distance of spots from the centre, with the closer pair having the minimal weight and the further pair the maximal weight.

$$w(n) = (n-1) \times 0.2, \qquad (4)$$

$$k(n) = \frac{w(n)}{\sum_i w(i)}$$

The resulting k is:

$$k = [0, \ 0.06, \ 0.13, \ 0.2, \ 0.26, \ 0.33] .$$

The asymmetry indices range from minus one to one, with positive values indicating a stronger response on the preferred side, and negative values indicating a stronger response on the null side.

Phase analysis. Response phases were detected based on threshold crossing, determined as 2 or 4 SD above baseline, for the spiking and synaptic inputs analysis, respectively. For both spiking and synaptic inputs, responses were separated into phases based on the local maxima, averaged over responses in all directions. Baseline activity was determined based on 500 ms before onset of bars. Local maxima with <10 spikes were excluded from the analysis, and phases <30 ms apart were combined. The DSI of each phase was determined as described above, with the preferred direction determined by a cell recorded within the same retinal piece before light adaptation. Then, the phases were assigned as 'On', 'Delayed On', 'Off' and 'Delayed Off' according to their timing, in fixed windows that matched the location of the bar.

The difference in the time of excitatory and inhibitory response onset was calculated by matching each excitatory phase with the closest inhibitory phase. Only pairs of phases that were <100 ms apart were included in the analysis. Response onset was determined as the time the response reached 20% of the peak.

For arithmetic summation of the synaptic inputs to a DSGC, we summed the average normalized currents (Brombas et al., 2017). In order to compare the results with the spiking output, the summation waveform was multiplied by minus one to account for the negative polarity of excitation.

In MEA recordings, the preferred direction of each cell was defined based on its response to gratings. Baseline activity was determined based on 500 ms before bar onset. Given that the MEA technique allows for the simultaneous recording of spatially distributed neurons, the entrance of the moving bar (and its departure) into the receptive field of a retinal ganglion cell depends on the location of the cell. Thus, in order to align and average responses evoked by the stimulus moving in all directions, we first estimated the centre of the receptive field based on the white-noise stimulus, then calculated any activity evoked from the time when the leading edge of the bar was 500 μm away from the receptive field centre until the time when the trailing edge was 500 μm away from the centre. To determine the receptive field centre of retinal ganglion cells, the spike-triggered average (STA) from the white-noise data was calculated by averaging the images that were presented in the 500 ms preceding each spike. From the STA, we extracted the stimulus frame with the highest peak-to-peak amplitude and fitted a two-dimensional Gaussian to the spatial component of the receptive field. We then defined the receptive field diameter of retinal ganglion cells as 2 SD of the two-dimensional Gaussian fit and the receptive field centre. For Fig. A7, cut-offs between phases were defined by fixed time points because the delayed On phase detection in the black on grey bar was limited by the trial duration (On and Off phase duration, 700 ms; delayed On phase, 600 ms).

Statistics. For the statistical analysis, data sets were tested for normality using a χ^2 goodness-of-fit test. Data sets that followed a normal distribution were compared using a two-sample Student's unpaired or paired t test, according to the data structure, and the Wilcoxon rank sum test was used for abnormally distributed data sets. When more than two groups were compared, one-way ANOVA was performed for normal distributions and Kruskal–Wallis test for abnormal distributions. Throughout the figures, sample statistics and waveforms are expressed as the mean $\pm$ SD, unless specified otherwise (Supporting information).

RIGHTS LINK(>

Results

Light adaptation increases the receptive field of posterior-preferring DSGCs asymmetrically

To explore the level of dynamics in the receptive field of retinal ganglion cells, we performed two-photon targeted loose-patch recordings from pDSGCs in the mouse retina, while presenting static spots across the preferred–null axis to cells that were initially dark adapted, and after intensive light exposure with full-field stationary light illumination for several minutes (see Methods). We refer to the first condition as 'before light adaptation' and to the latter as 'light adapted'. To cover a sufficient number of excitatory synapses in the centre and surround, we increased the spot size with distance from the centre (Fig. 1A). We used the responses to the onset and offset of the spots to estimate the receptive field diameter of pDSGCs. Before light adaptation, On and Off receptive fields were restricted to spots that appeared within their dendritic arbor (~180 μm in diameter; Rivlin-Etzion et al., 2011) (Fig. 1A–C). Following light adaptation, both receptive fields increased significantly, and even spots located far in the surround of pDSGCs evoked spikes (Fig. 1A–C). This expansion was asymmetric towards the preferred side of the pDSGC, particularly for the On receptive field (Fig. 1D; asymmetry index On = 0.44; Off = 0.15). In both conditions, On receptive fields tended to be larger than Off receptive fields (Fig. 1C), and light adaptation led to an increase in the total number of spikes evoked in response to the stimulus, suggesting a sensitization of the cells (Fig. 1E) (Huang et al., 2022). Note that following light adaptation the response was not only stronger but also more sustained (On response duration before light adaptation, 305.00 ± 255.44 ms; after light adaptation, 779.33 ± 149.21 ms; $P = 1.96 \times 10^{-4}$; see Methods). Finally, the polarity preference of the cells also changed, because the On response became more dominant following light adaptation (Fig. 1E).

pDSGCs reveal multiple response phases to moving bars following light adaptation

To gain insight into the role of receptive field dynamics in computation of the direction of motion, we measured the directional tunings of pDSGCs before and after light adaptation. We used two different adaptation protocols [stationary light illumination, as in Fig. 1, and repetitive visual stimulation with moving gratings (RVS)]; both adaptive stimuli were presented for 3.0–5.5 min in photopic light levels (Fig. 2; see Methods). Previously, we showed that RVS can reverse the directional tuning of pDSGCs in response to drifting gratings that stimulate the centre and surround simultaneously (Ankri et al., 2020; Rivlin-Etzion et al., 2012). To separate the contribution of the centre and surround receptive fields to pDSGCs' directional tuning, we recorded their activity in response to bars that traverse across ~1 mm distance, sequentially stimulating the different receptive field subregions. The tuning sharpness was quantified by the DSI, calculated based on the responses in the original posterior preferred direction (i.e. before any light adaptation protocol). The DSI values ranged from one to minus one, indicating a stronger response in the original preferred direction or the null direction, respectively.

Before light adaptation, pDSGCs displayed transient and directionally tuned spiking activity to the leading (On response) and trailing (Off response) edges of the bars (Fig. 2A). Whether presented with moving bars or drifting gratings, pDSGCs exhibited the same directional preference (Fig. A1A and B). Following either stationary light illumination or RVS, several changes occurred in the response of pDSGCs. First, the overall number of spikes increased (Fig. 2A–C), in accordance with the increased spiking in response to static spots (Fig. 1E; Fig. A1C). Second, the polarity preference of pDSGCs shifted, from balanced On and Off responses overall to a more dominant On response, to the extent that the Off response was almost absent in some cells (Fig. 2B–F). This polarity shift is in accordance with the change in the On/Off response ratio to static spots following light adaptation (Fig. 1E). Considering the diminished Off response, we focused the analysis below on the On response.

Following either light adaptation protocol, the overall response to the moving bars lost its directional preference and the DSI decreased (Fig. 2B–E; Fig. A1D–F). The response of pDSGCs exhibited a more complex pattern, with multiple distinct phases. Interestingly, these phases were often oppositely tuned, with the initial response to the leading edge of the bars tuned to the original preferred direction, and the additional delayed phase (referred to as 'delayed-On' phase) tuned to the null direction (Fig. 2B and C; Fig. A1E). Following RVS, even pDSGCs that displayed high DSI values in response to gratings showed reduced DSI values in response to bars, indicating the emergence of the oppositely tuned delayed-On phase in these cells (Fig. A1F). Conversely, the persistent preferred-direction response in the early phases following light adaptation explains why pDSGCs, including cells that displayed negative DSI values in response to gratings, never reversed fully in response to bars (Fig. A1E and F). The shift in polarity preference of pDSGCs and the null-tuned delayed phase occurred simultaneously following both types of light adaptation, as indicated by the negative correlation between the DSI and the On/Off response ratio (Fig. 2D and E). Thus, either protocol of light adaptation (stationary light and RVS) induces fundamental changes in the response properties of pDSGCs, in terms of receptive field size, polarity preference and directional tuning.

Null-tuned delayed responses are spatially correlated with activity in the surround of pDSGCs

To correlate the changes in the receptive field size with the directional response to moving bars, we estimated receptive fields of pDSGCs by aligning their spiking responses to the location of moving bars (Fig. 3*A* and *B*; see the Methods). We refer to this receptive field approximation as the 'motion receptive field'. Whether
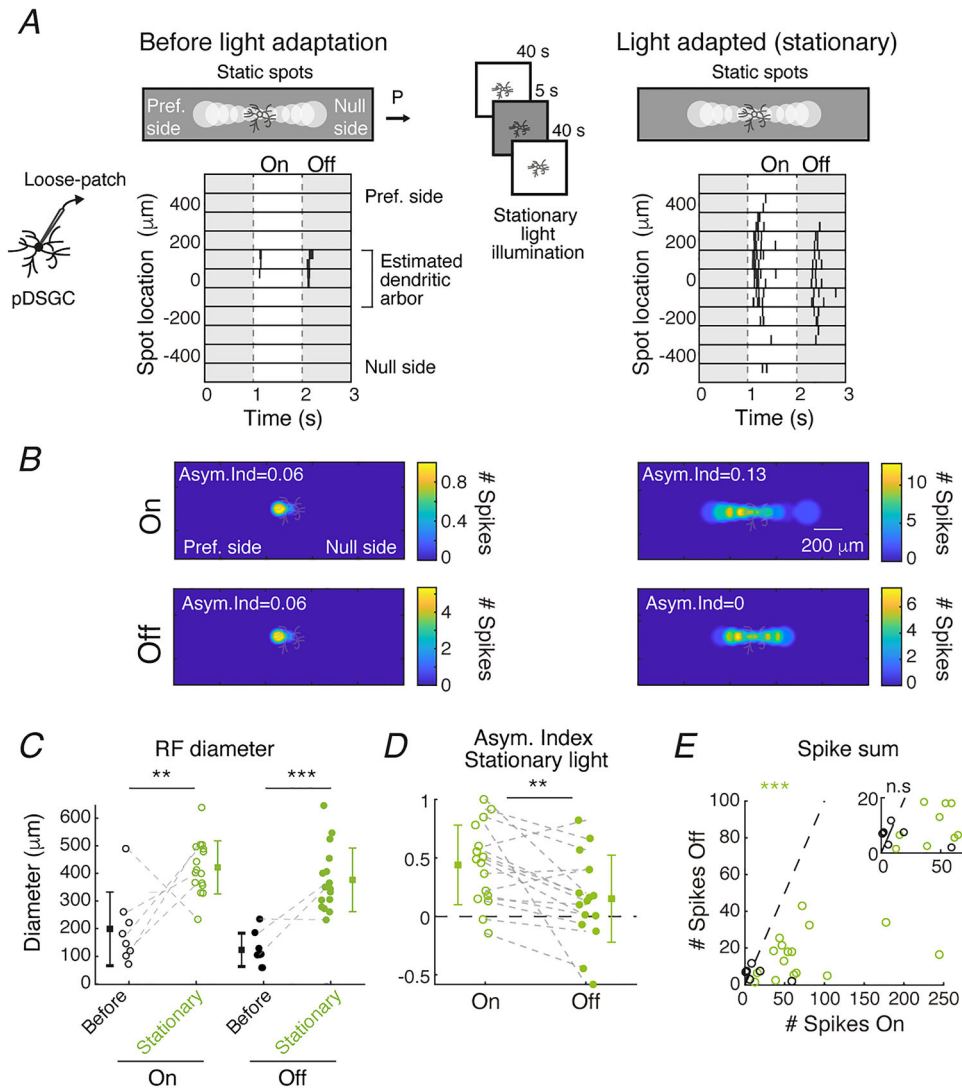

Figure 1. Light adaptation asymmetrically increases receptive field of posterior-preferring direction-selective ganglion cells

A, responses of an example posterior-preferring direction-selective ganglion cell (pDSGC) to static spots of different radii presented in the preferred–null axis (illustrated at the top), before (left) and after (right) light adaptation with stationary light illumination. The posterior direction is marked by an arrow. Each line in the raster plot illustrates the spiking activity in two repetitions of the stimulus in each location. The cell soma is located at zero; negative values denote distances in the null side, positive values in the preferred side. *B*, the On (top) and Off (bottom) receptive fields calculated from the response to the static spots in *A*. Asymmetry indices are denoted on top. *C*, On and Off receptive field diameter before (black) and after (green) light adaptation with stationary light. Dashed lines connect values of the same cells (before: $n = 10$, two cells had no On response and three had no Off response; stationary light: $n = 16$; $P_{On} = 0.002$; $P_{Off} = 0.0001$). The means ± SD are shown next to the values. *D*, the On (open circles) and Off (filled circles) asymmetry indices of all cells recorded following stationary light illumination ($P = 0.0045$). *E*, total number of spikes during onset *vs.* offset of spots for all cells recorded before (black) and after (green) stationary light illumination. Inset is a zoom-in. Green stars denote the *P*-value for the difference between On and Off spikes after stationary light illumination ($P = 0.0004$); black (n.s.) is for cells before light adaptation. Student's *t* test, **$P < 0.01$ and ***$P < 0.001$. Abbreviations: Asym. Ind, asymmetry index; P, posterior; pDSGC, posterior-preferring direction-selective ganglion cell; RF, receptive field; Pref. side, Preferred side.
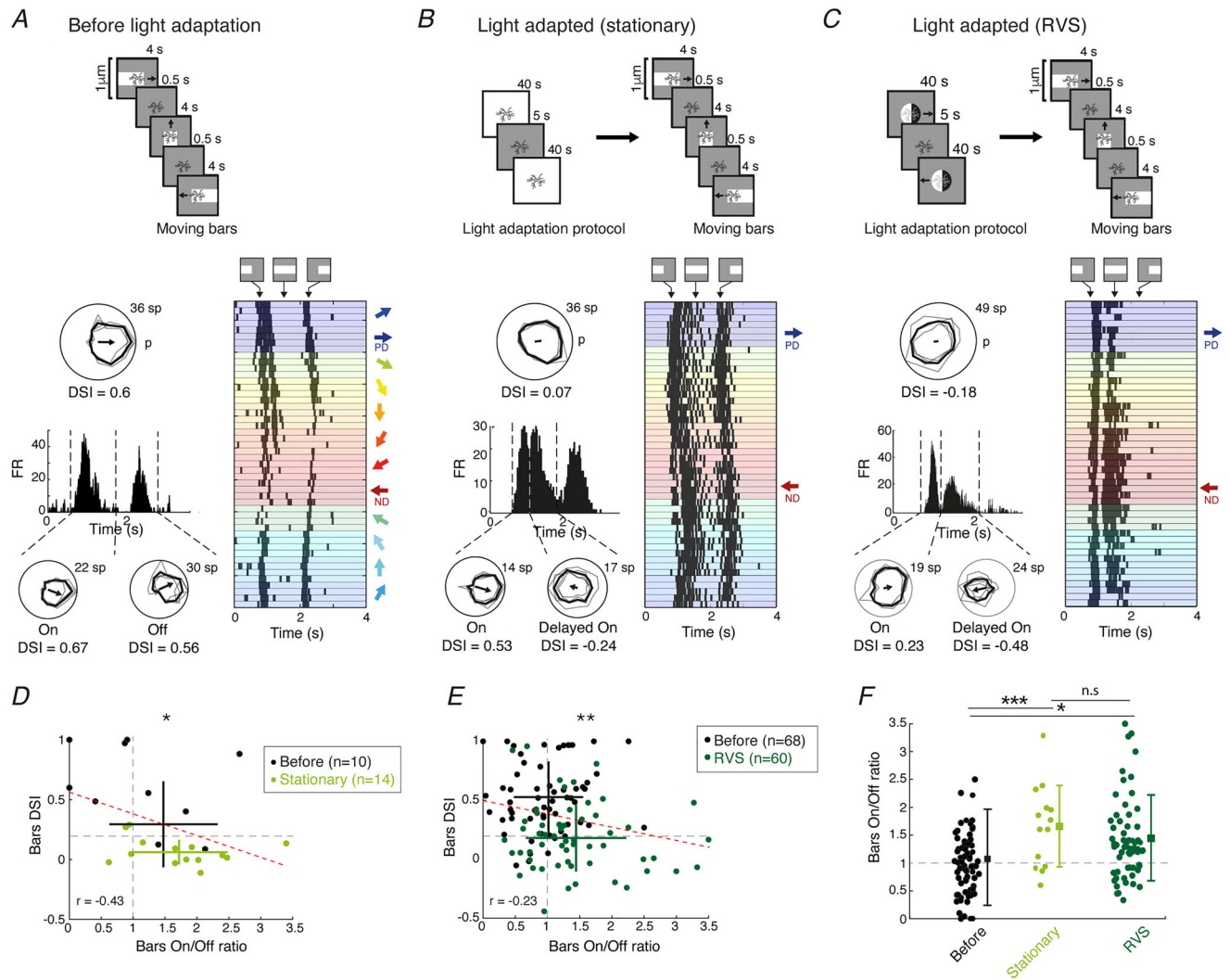
Figure 2. Different types of light adaptation expose oppositely tuned response phases in posterior-preferring direction-selective ganglion cell spiking activity in response to moving bars

A, top, illustration of the moving bar stimulation (12 directions; 4 repetitions). *A*, left, polar plot of the directional tuning of an example pDSGC in response to the moving bars (black bold line, mean; grey line, single repetition). Peristimulus time histograms (PSTHs; 10 ms bin) averaged over all directions. Dashed lines separate the detected response phases. Bottom polar plots show the directional tuning for each response phase. A, right, raster plot showing the spiking activity of the cell in response to moving bars, colour coded by direction, each repeated four times. The position of the bar at several time points is illustrated on top. *B* and *C*, same as in *A*, but for a cell after light adaptation by stationary light illumination (*B*) or RVS (*C*). Before light adaptation and RVS, examples are recorded from the same cell. *D*, the DSI calculated in response to moving bars *vs.* the On/Off response ratio, before and after light adaptation with stationary light. The regression line is shown in red (the two conditions are pooled and regressed together); regression value is noted at the bottom; asterisks denote the significance level and refer to the regression line ($P = 0.03$). The mean ± SD is shown for both populations. Vertical and horizontal dashed lines indicate equal On and Off responses and DSI = 0.2, respectively. The number of cells in each condition is in the key. *E*, same as in *D*, but for cells before and after light adaptation with RVS ($P = 0.01$). *F*, comparison of the On/Off response ratio of all cells in all conditions during bar presentation ($P_{\text{before-RVS}} = 0.01$; $P_{\text{before-stationary}} = 6.7 \times 10^{-3}$; $P_{\text{stationary-RVS}} = 0.36$). Dashed line indicates equal On and Off responses. Kruskal–Wallis test, $*P < 0.05$, $**P < 0.01$ and $***P < 0.001$. Abbreviations: DSI, direction-selective index; p, posterior; PD, preferred direction; ND, null direction; pDSGC, posterior-preferring direction-selective ganglion cell; PSTH, peristimulus time histogram; RVS, repetitive visual stimulation; sp, spikes.

recorded before or after light adaptation, the motion receptive field was bigger than the static receptive field, as calculated from the response to static spots (Fig. 3*C*). Similar to the static receptive field (Fig. 1), the motion receptive field of pDSGCs expanded following light adaptation (Fig. 3*C* and *D*). The calculated receptive field diameter was negatively correlated with the DSI, suggesting a link between the extent of surround expansion and the strength of the delayed null-tuned response phase (Fig. 3*E*).

To confirm the link between receptive field size and direction selectivity, we plotted the average peristimulus time histograms (PSTHs) in response to the moving bars in all 12 directions (Fig. 4*A*). For this analysis, we included cells in the light-adapted condition only if they had a DSI $\leq$ 0.2 (i.e. 'stable' cells were removed; 37/64

cells following RVS and 12/15 cells following stationary light illumination passed the criteria for inclusion; see DSI cut-off in Fig. 2*D* and *E*). Before light adaptation, the On response of pDSGCs occurred when the leading edge of the bar crossed the dendritic arbor of the cell, whereas following light adaptation, the response was less confined temporally and persisted when the bar hit the surround receptive field (Fig. 4*A*, grey areas). To determine the directional tuning of distinct response phases, we identified local maxima in the PSTH of individual pDSGCs and plotted their DSI values as a function of peak time (see Methods). Before light adaptation, both On and Off phases displayed high DSI values ($DSI_{on} = 0.7 \pm 0.25$; $DSI_{off} = 0.65 \pm 0.3$; mean $\pm$ SD; $n = 38$). Following light adaptation, the main On response phase still exhibited a positive DSI value, but
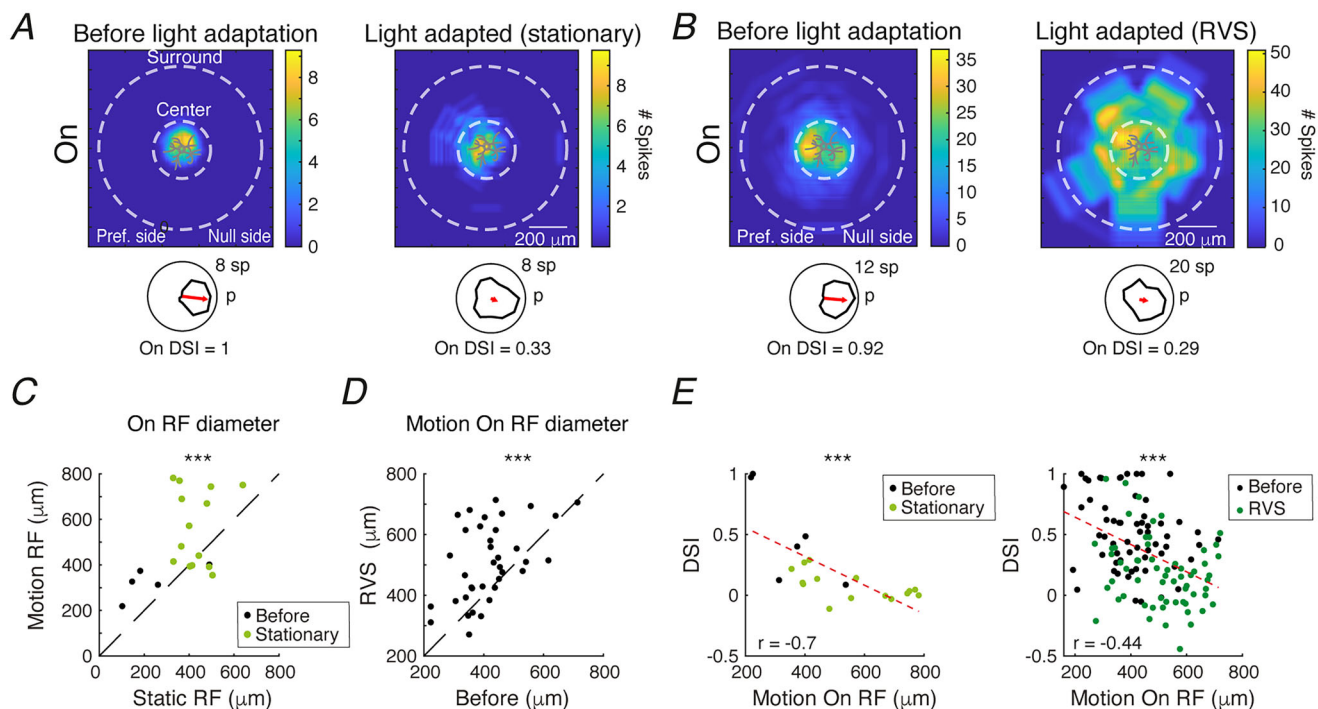

Figure 3. Receptive field expansion of posterior-preferring direction-selective ganglion cells following light adaptation is reflected in their response to moving bars
A, the motion receptive field for an example pDSGC, constructed by aligning the responses to the leading edge location of the bar (On response) in 12 different directions before (left) and after (right) light adaptation with stationary light illumination. *B*, same as *A* for RVS. Estimated centre and surround regions are marked by the dashed circles. The number of spikes is colour coded; the scale is on the right. Below each receptive field, the polar plots of the On responses (both early and delayed phases combined) are plotted, with the maximum number of spikes denoted on the outer circle. The DSI value of the response is below each polar plot. *C*, motion *vs.* static receptive fields before (black) and after (light green) light adaptation with stationary light illumination. Asterisks denote the statistical significance of the difference between motion and static RF size (pooled across conditions; $P = 0.009$). *D*, the motion On receptive field diameter following RVS *vs.* before light adaptation ($P = 7 \times 10^{-5}$). *E*, the DSI in response to bars before and after light adaptation with stationary light illumination (left) or RVS (right) plotted against the On motion receptive field diameter. The dashed red line is the fit of the data points from both conditions; the correlation coefficient (*r*) is denoted at the bottom left. Asterisks denote the significance level of the regression line ($P_{before-stationary} = 2.6 \times 10^{-4}$; $P_{before-RVS} = 1.9 \times 10^{-7}$). *C* and *D*, Student's paired *t* test; *E*, regression analysis. ***$P < 0.001$. Abbreviations: DSI, direction-selective index; p, posterior direction; pDSGC, posterior-preferring direction-selective ganglion cell; RF, receptive field; RVS, repetitive visual stimulation.
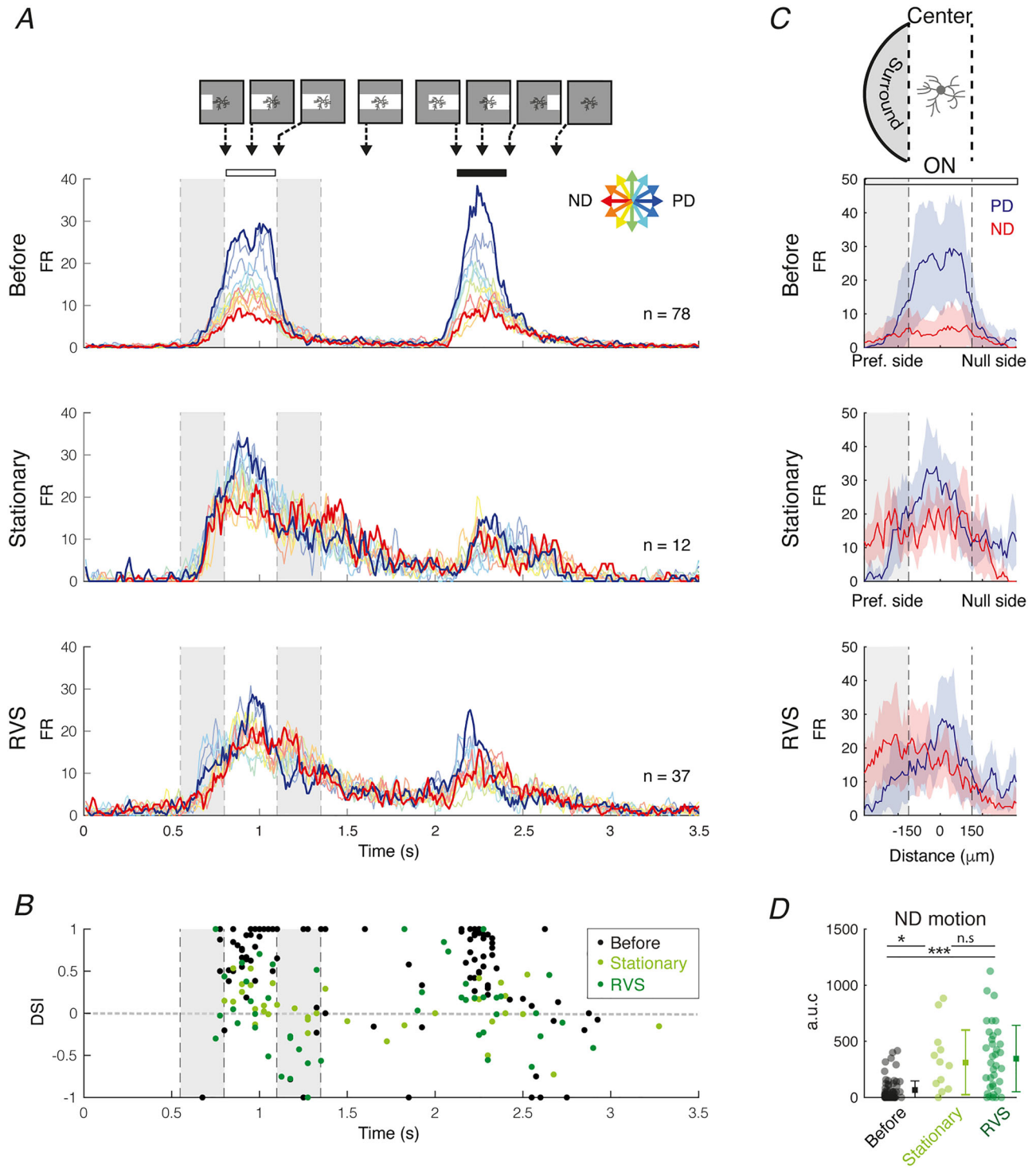
Figure 4. Light adaptation strengthens null-tuned responses in the preferred side surround of posterior-preferring direction-selective ganglion cells

A, PSTH of average directions in response to moving bars before (top) and after light adaptation with stationary light illumination (middle) or RVS (bottom), colour coded by the angular distance from the preferred direction (top right). The number of cells in each condition is denoted. The location of the bar during motion in the preferred direction is illustrated relative to the cell at several time points. Vertical grey boxes indicate the time when the leading edge of the bar traverses the surround receptive field, and horizontal white and black stripes above the waveforms denote the estimated time when the leading and trailing edges traverse over the dendritic arbor of the cell, respectively.

B, DSIs of the detected response phases in all cells plotted against the time of phase peak. Horizontal dashed line marks DSI = 0. Phases detected in the different conditions are overlaid and colour coded. Each cell can be represented by multiple dots, according to the number of detected phases. *C*, top, illustration of a pDSGC and the preferred side surround receptive field (grey area); bottom, normalized PSTH (mean ± SD) during preferred and null motion plotted against the location of the leading edge of the bar (On) relative to the cell in all three conditions (soma is located at $x = 0$). *D*, the a.u.c. (mean ± SD) over the preferred side surround (grey area), calculated on the PSTH during null direction motion. ($P_{\text{before-RVS}} = 3.6 \times 10^{-5}$; $P_{\text{before-stationary}} = 0.03$; $P_{\text{stationary-RVS}} = 0.5$; one-way ANOVA). Kruskal–Wallis test, *$P < 0.05$ and ***$P < 0.001$. Abbreviations: a.u.c., area under the curve; DSI, direction-selective index; ND, null direction; PD, preferred direction; pDSGC, posterior-preferring direction-selective ganglion cell; PSTH, peristimulus time histogram; RVS, repetitive visual stimulation; FR, firing rate.

the additional delayed phases showed reduced DSI values that were often negative, indicating null-tuned responses, especially following RVS (Fig. 4*B*).

To better align the directional response to the location of the bar, and thereby to the changes in the receptive field, we replotted the PSTH for preferred and null directions, this time as a function of the location of the bar with respect to the cell soma. We focused on 360 μm from each side of the cell, including both the centre and surround (Fig. 4*C*; see Methods). In all conditions, the main On response of pDSGCs was stronger in the preferred direction and occurred when the leading edge of the bar traversed its centre receptive field. After light adaptation, and when the leading edge of the bar traversed the preferred side surround (a region >150 μm from the soma of the cell), the response of pDSGCs was stronger in the null direction (grey area in Fig. 4*A* and *C*). To quantify the activation of this null-tuned surround across the different conditions, we calculated the area under the curve (a.u.c.) of the null direction PSTH obtained in response to the bar traversing this region. The null direction surround activation strengthened following light adaptation with stationary light illumination, and even more so following RVS (Fig. 4*D*). Taken together, these data show that light adaptation enhances the activation in pDSGCs in their preferred side surround receptive field and that this activity is tuned to the null direction. Although both forms of adaptation exposed null-tuned activation in this region, it appears to be stronger following RVS, suggesting that RVS is a more efficient form of light adaptation than stationary light illumination, probably owing to the fact that it alternates continuously between On and Off and activates the two pathways intermittently.

The data presented thus far were collected in response to high-photopic light adaptation protocols, where the adaptive stimulus is presented to a restricted region around the cell soma (300 μm in diameter). To test whether the emergence of the surround-mediated null-tuned response depended on the light intensity of the adaptive stimulus or its spatial extent, we presented pDSGCs with full-field RVS (~1 mm diameter) at 10-fold lower light intensity. The dynamics of light adaptation in pDSGCs were consistent, appearing even in photopic light intensities and independent of the spatial extent of light adaptation (Fig. A2).

Although we assumed that the null-tuned delayed phase originates from the surround of pDSGCs, a similar effect could emerge from a time-fixed delayed excitation, which is independent of the location of the bar. To test this, we presented pDSGCs with bars moving at three different speeds (Fig. 5*A*). As shown above, before light adaptation the phases detected were bound to the centre receptive field, whereas following RVS additional phases occurred in all three speeds (Fig. 5*B*). The time of the delayed phase changed with the speed of movement of the bar and corresponded to the location of the bar (Fig. 5*C*), demonstrating that the response originated from the preferred side surround activation and not from the temporal characteristics of the response following adaptation.

To isolate the contributions of the centre and surround receptive field to the response of pDSGCs, we presented them with moving bars selectively activating either their centre or surround receptive fields, by masking one or the other (Fig. A3*A*). Before light adaptation, the response originated exclusively from the centre receptive field, evident in the almost complete ablation of the response when masking the centre, whereas masking the surround had only a minor effect on the response (Fig. A3). Following light adaptation with stationary light illumination, the surround became significantly more prominent (Fig. A3). Summing the centre and surround traces in both conditions recapitulated the response to the globally moving bars (Fig. A3*C*), suggesting a linear summation of the response across the receptive field. Taken together, these results confirm that the null-tuned delayed On response emerges from surround activation of pDSGCs following light adaptation.

Null-tuned responses from the surround receptive field of pDSGCs are mediated by excitation

To understand the circuit components underlying receptive field changes of pDSGCs following light adaptation, we recorded their synaptic inputs during the presentation of bars moving in the preferred and null directions. Before light adaptation, null motion inhibition was stronger and faster than preferred motion inhibition (Fig. 6*A* and *B*; Fig. A4*A*). These observations were previously reported and are expected from the centrifugal

preference of SACs and from the asymmetric inhibition they provide to DSGCs (Ankri et al., 2020; Briggman et al., 2011; Chen et al., 2016; Euler et al., 2002; Fransen & Borghuis, 2017; Wei et al., 2011; Yonehara et al., 2011). To quantify the directional tuning of inhibitory and excitatory phases, we identified local maxima in the current waveforms and plotted the DSI values against the time of the detected phases (see the Methods). Inhibition ruled the directional response to bars before light adaptation, as quantified by the negative DSIs for both the On and Off phases (Fig. 6*C*; On-DSI_{Inh} = -0.48 ± 0.3; Off-DSI_{Inh} = -0.5 ± 0.4; mean $\pm$ SD). Off, but not On, excitation tended to be directionally tuned to the preferred direction (On-DSI_{Exc} = 0.08 ± 0.3; Off-DSI_{Exc} = 0.2 ± 0.4; mean $\pm$ SD), suggesting that unlike the On response,

the Off response tuning relies on both inhibitory and excitatory mechanisms.

Light adaptation with RVS led to substantial changes in the inputs to pDSGCs. Given that, as shown above for the spiking activity, the Off inputs were significantly reduced, the analysis below is focused on the inputs during the On phase. We found that the inhibition was no longer directional (Fig. 6*A* and *D*), demonstrated by DSI values that clustered around zero (Fig. 6*E*; On-DSI_{Inh} = -0.1 ± 0.2; mean $\pm$ SD), and that the timing of inhibition during the null direction no longer preceded excitation (Fig. A4*A*). The evident complex response in the spiking activity (Figs 2 and 4) was reflected in the excitatory inputs, with the early phases tuned to the original preferred direction and the delayed ones to the null direction
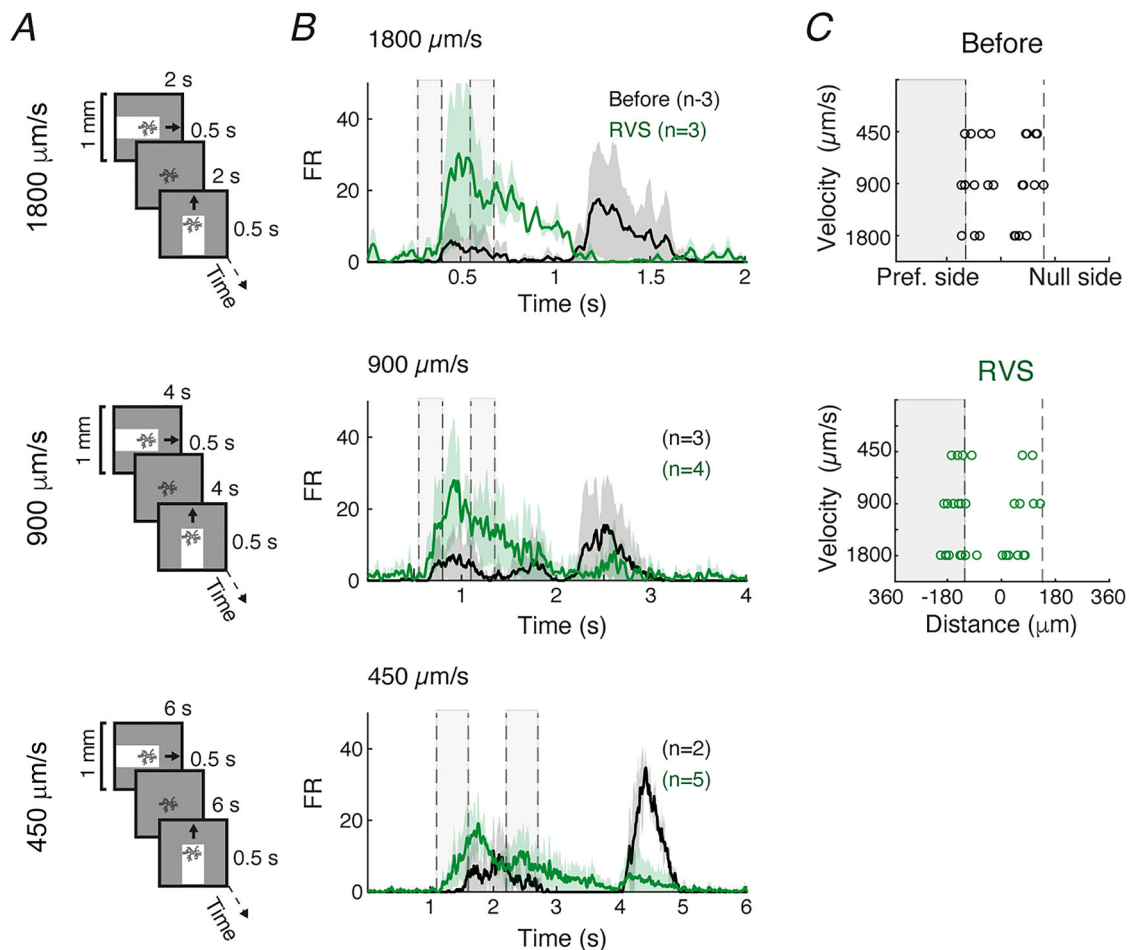

Figure 5. The spatial correlate of the delayed-On response phase is independent of the bar's velocity
A, illustration of the moving bars presented to pDSGCs at three different velocities: 1800 µm/s (top), 900 µm/s (middle) and 450 µm/s (bottom). *B*, PSTH (mean $\pm$ SD) of pDSGCs recorded in response to bars averaged across directions, before and after light adaptation with RVS, for the three different velocities. The number of cells recorded in each condition is in parentheses. Dashed lines indicate the location of the bar, as in Fig. 4. *C*, the time of the peak of detected phases from PSTH responses is plotted against the distance from cell soma (*x* = 0) for each velocity, before RVS (black, top) and after RVS (green, bottom). Notations are as in Fig. 4*C*. There was no significant difference in the time of phase occurrence across velocities (P_{DA} = 0.74; P_{RVS} = 0.93; Kruskal–Wallis test). Abbreviations: FR, firing rate; pDSGC, posterior-preferring direction-selective ganglion cell; PSTH, peristimulus time histogram; RVS, repetitive visual stimulation.
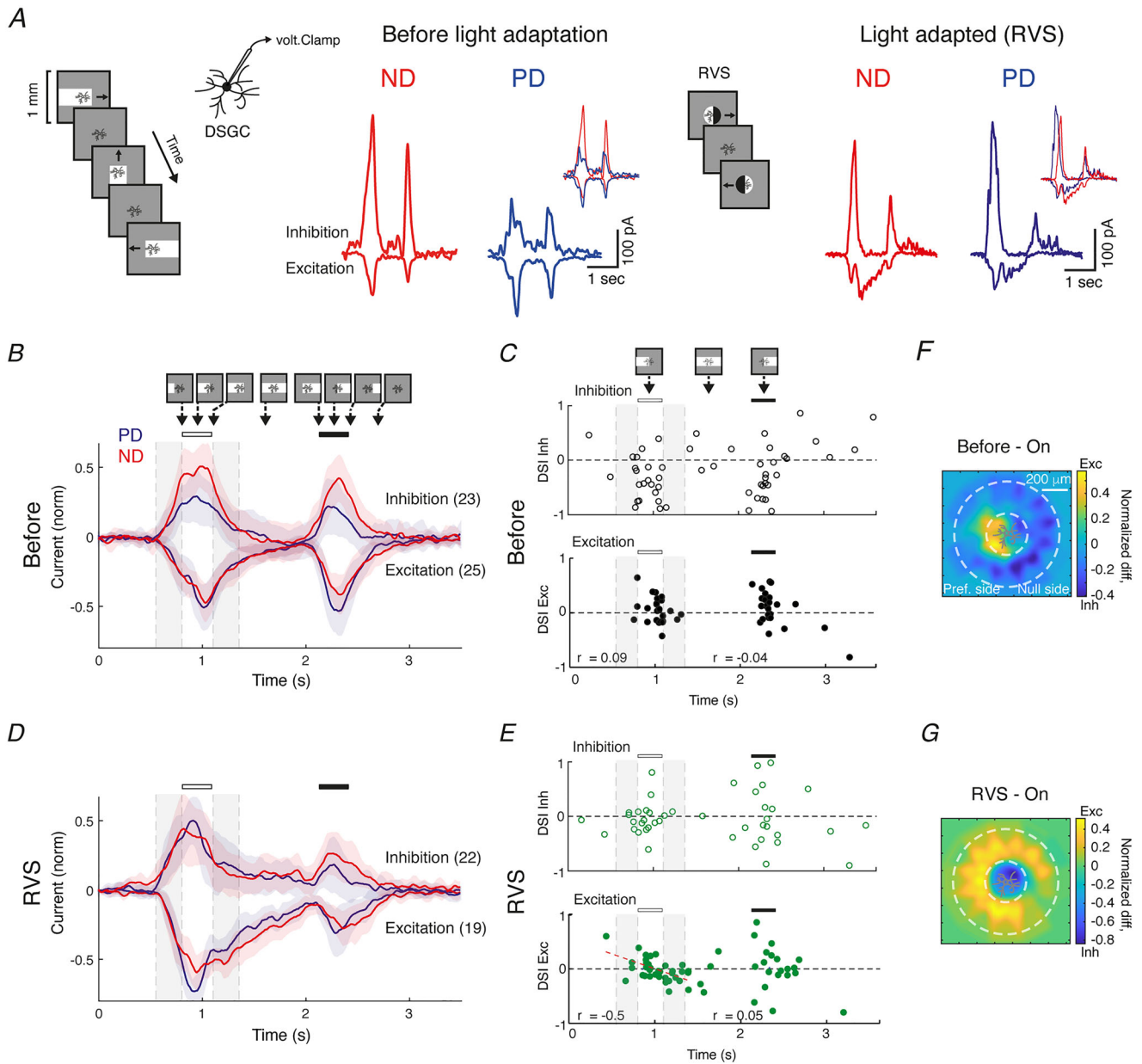
Figure 6. Surround excitation underlies null-tuned delayed-On phase of posterior-preferring direction-selective ganglion cells

A, voltage-clamp recordings of an example pDSGC in response to bars (stimulus on the left) moving in the preferred direction (PD; blue) and null direction (ND; red) before (left) and after (right) light adaptation with RVS. Currents are averages of four repetitions. Inset, the ND and PD superimposed. *B*, average of the normalized inhibitory and excitatory currents (mean ± SD) in the response of pDSGCs to bars moving in the preferred and null directions. The number of cells recorded at each voltage is in parentheses. An illustration of the location of the bar relative to the cell at several time points is shown at the top. Vertical grey boxes and horizontal white and black stripes are as in Fig. 4. *C*, DSI of distinct response phases of inhibition (top) and excitation (bottom), for all cells recorded before light adaptation, plotted against time of phase peak. The location of the bar is illustrated relative to the cell at three time points. Grey boxes and white and black horizontal lines are as in *B*. Horizontal dashed line denotes DSI = 0. Excitation currents of On and Off periods were fitted separately, and their correlation values are denoted at the bottom. *D* and *E*, as in *B* and *C*, but for cells after light adaptation with RVS. *F* and *G*, the average normalized On motion receptive field of pDSGCs before (*F*) and after (*G*) light adaptation with RVS, constructed from the arithmetic summation of the inhibitory and excitatory current. For this analysis, a subset of cells that were recorded in response to bars moving in 12 directions were used (n_{DA} = 7 cells; n_{RVS} = 5 cells). Positive values denote locations where excitation is stronger than inhibition, and vice versa for negative values. The illustration of a cell in the centre denotes the estimated location of the recorded pDSGC in relationship to the locations of bars.

Abbreviations: diff, difference; DSI, direction-selective index; Exc, excitation; Inh, inhibition; ND, null direction; PD, preferred direction; pDSGC, posterior-preferring direction-selective ganglion cell; RVS, repetitive visual stimulation.

(Fig. 6*D* and *E*). To quantify this trend, we linearly fitted the DSI values of the excitatory phases. We found that following RVS, On-excitation DSI displayed a negative regression slope and a higher correlation coefficient than the other phases [slope = −0.6 (DSI/s); r_{On} = −0.5; Fig. 6*D*].

To link these data to the change in the receptive field, we calculated the motion receptive field as in Fig. 3, but this time from the summed potentials. In dark adaptation, excitation dominated the centre of the response, with a slight shift towards the preferred side, whereas inhibition dominated the null side (Fig. 6*F*). This receptive field shape is expected from SACs null side inhibition and the spatial asymmetry of excitatory inputs towards the DSGC preferred side (Ding et al. 2021). Following RVS, the motion receptive field for the summed potentials expanded dramatically, mostly towards the preferred side and the least on the null side (Fig. 6*G*). To obtain a better understanding of the spatial changes in the inputs to pDSGCs, we compared the inhibitory and excitatory receptive fields separately. The results show that pDSGC surround excitation strengthened following RVS, as did centre inhibition (Fig. A4*B*). These results are in line with the data from the masking experiment, in which the centre activation is dramatically reduced following RVS (Fig. A3), possibly owing to enhanced surround suppression. To confirm that the currents to pDSGCs reliably reflect their spiking activity, the normalized excitatory and inhibitory potentials were linearly summed, and the resulting waveforms in the preferred and null directions were superimposed. The shape of the summed potentials matched the shape of the spiking activity, displaying a clear null-tuned delayed phase (Fig. A4*C* and *D*).

To summarize, these data suggest that the excitatory receptive field of pDSGCs expands following light adaptation asymmetrically, skewed towards the preferred side of the cells. Additionally, these surround-mediated inputs are tuned to the null direction, exhibiting an intriguing example of directionally tuned excitation to pDSGCs.

Pharmacological manipulations expose the role of inhibitory players and the On pathway in mediating activity shifts following light adaptation

The spatial shifts in the excitatory inputs of pDSGCs following light adaptation suggest the involvement of feedback and lateral inhibition in bipolar cells (Chávez et al., 2010; Franke et al., 2017; Huang et al., 2022; Roska et al., 2000; Strauss et al., 2022; Zhang & Wu,

2009). In addition, excitation from bipolar cells was shown to carry directional information that is mediated by feedback inhibitory circuits (Matsumoto et al., 2021). We, therefore, searched for possible involvement of inhibitory players in mediating the null-tuned excitatory surround. Application of the $GABA_A$ receptor blocker SR95531 (gabazine; 10 μM) before light adaptation led to an increase in the firing rate of pDSGCs in both preferred and null directions and exposed a delayed spiking phase, corresponding to increased activity in the surround in all directions (Fig. 7*A* and *B*). Application of the glycinergic receptor blocker strychnine (1 μM) following RVS had the opposite effect on pDSGCs; the null-tuned surround-mediated response was reduced (Fig. 7*C* and *D*). These results suggest that the surround-mediated excitation to pDSGCs relies on an interplay between GABAergic and glycinergic inhibition, which have opposite effects on the delayed-On response phase.

As mentioned above, the change in the response of pDSGCs to moving bars following light adaptation was accompanied by a decrease in the Off inputs to the cells, suggesting shifts in the contribution of the On and Off pathways. To elucidate the involvement of On and Off pathways in the emergence of the null-tuned delayed On phase, we blocked the On-pathway inputs to pDSGCs before and after light adaptation with RVS using bath application of the metabotropic glutamate receptor agonist L-2-amino-4-phosphonobutyric acid (L-AP4; 20 μM). Although L-AP4 completely blocked the On response in cells before light adaptation, following RVS we noticed a residual On phase in the cells (Fig. A5). The remaining On response was small and insufficient to be considered as the main contributor to the delayed phase. We conclude that the delayed On phase is mediated primarily by the On pathway, and a possible minor contribution might come from an increase in the interaction between the On and Off pathways following RVS.

Null-tuned delayed phase occurs in all DSGC subtypes

We next investigated whether the response phase detected in pDSGCs is a general motif in the computation of motion direction in the retina. To answer this, we analysed pre-existing data from MEA retinal ganglion cell recordings, in which the retina was exposed to various visual stimuli for 9.44 ± 11.6 min (mean ± SD) in the low photopic regime prior to presentation of moving bars. We determined the polarity preference of cells according to their response to static full-field light stimulation,

identified DSGCs according to their responses to moving gratings (Fig. A6*A* and *B*) and divided them into sub-populations according to their polarity preference and cardinal direction preference (Oyster & Barlow, 1967; Sabbah et al., 2017). We separated the averaged responses into distinct response phases as before (Fig. 2) and measured their DSI values. In 44% of the On–Off DSGCs, we found the emergence of a delayed-On response phase after the initial On response; the delayed-On response tended to be directionally tuned to the null direction of DSGCs, evidenced by the negative DSI values (Fig. 8*A–D*).

To establish statistical significance of the tuning of the delayed-On phase towards the null direction, we tested the DSI distribution against the DSI of the baseline activity of cells, before the arrival of the bars in the receptive field of the cells. We found that the DSI values of delayed-On phases differed significantly from those measured during baseline activity (Fig. 8*D*; baseline DSI, 0.08 ± 0.49; Del-On DSI, -0.14 ± 0.36; mean $\pm$ SD; $P = 0.0015$). Histograms of the deviation from the preferred direction (determined by the response to moving gratings) show that although the On and Off phases
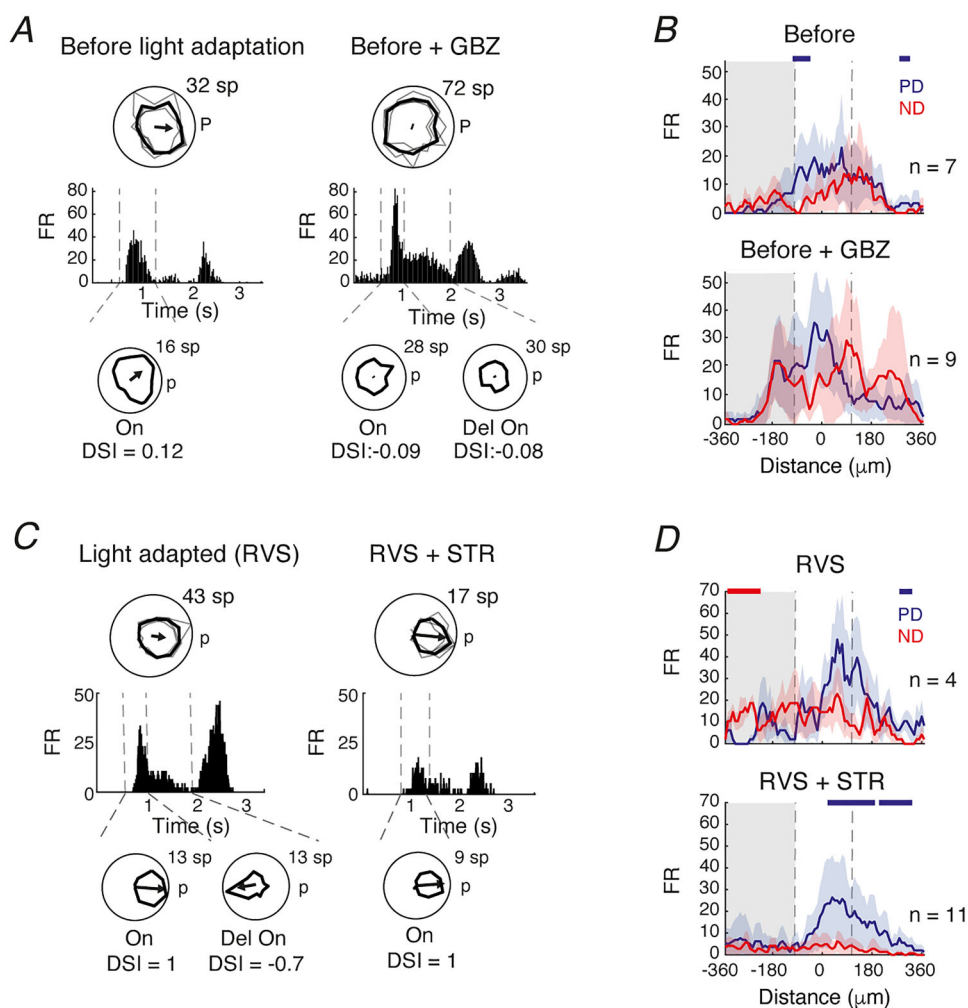

Figure 7. Gabazine and strychnine have opposite effects on the null-tuned delayed-On phase of posterior-preferring direction-selective ganglion cells

A, polar plot and PSTH of an example pDSGC spiking response to moving bars before light adaptation, prior to (left) and following (right) the application of GBZ. Polar plots at the bottom denote the directional tunings of separated phases (separated by dashed lines). *B*, population PSTH (mean $\pm$ SD) during motion in the preferred direction (PD, blue) and the null direction (ND, red) plotted against the location of the leading edge of the bar relative to the cell (soma is located at $x = 0$) before (top) and after (bottom) GBZ application. Coloured horizontal bars above the traces denote bins in which one of the traces is significantly higher ($P < 0.05$) than the other (blue for PD; red for ND). *C* and *D*, same as in *A* and *B*, but for cells after RVS and application of STR. Abbreviations: FR, firing rate; GBZ, gabazine; ND, null direction; p, posterior direction; PD, preferred direction; pDSGC, posterior-preferring direction-selective ganglion cell; PSTH, peristimulus time histogram; RVS, repetitive visual stimulation; sp, spikes; STR, strychnine.
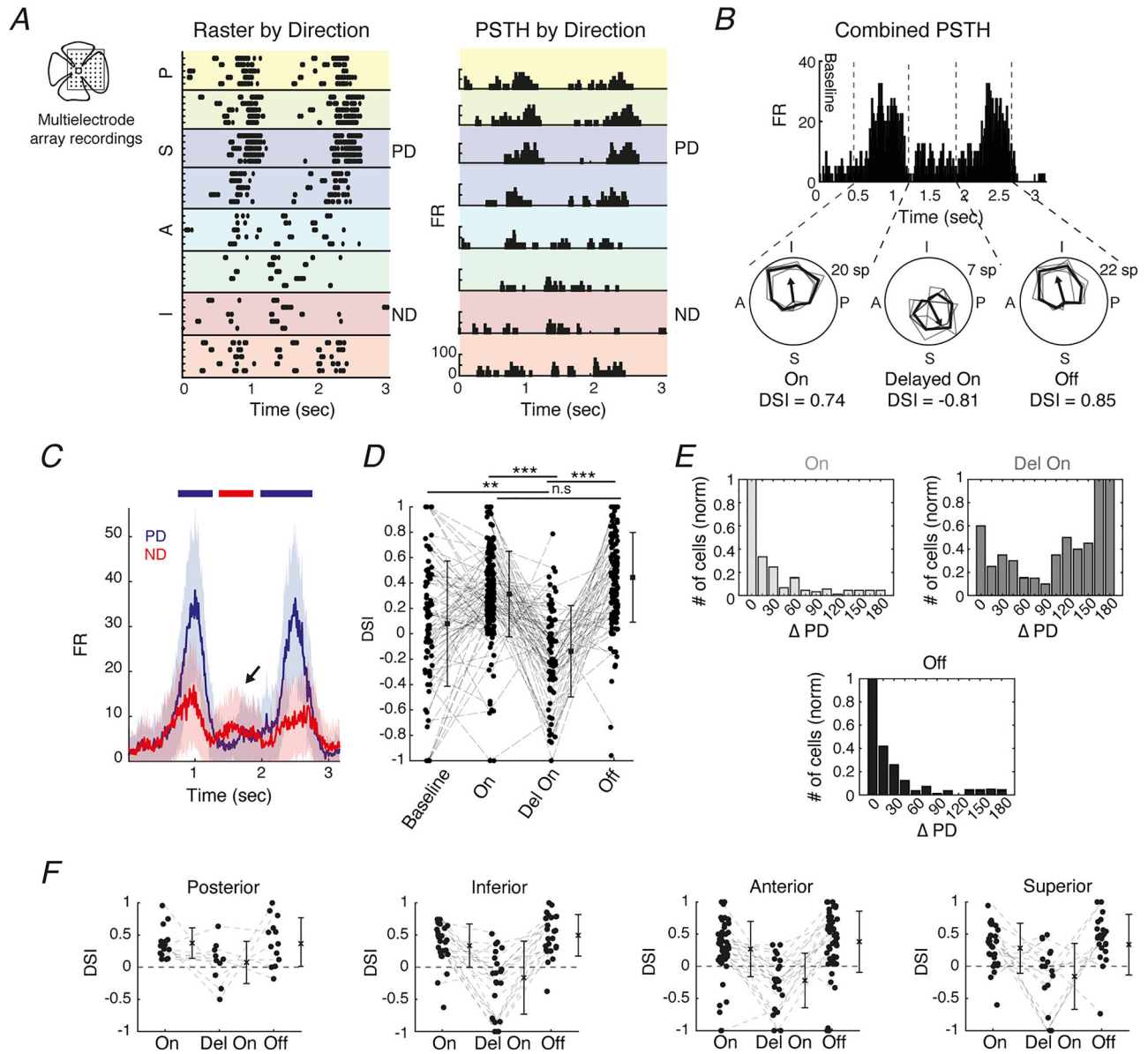
Figure 8. Multi-electrode array recordings reveal that the null-tuned, delayed-On phase occurs in all subtypes of direction-selective ganglion cells

A, raster plot (left) and PSTH (right) of an example superior-preferring DSGC presented with bars moving in eight directions, recorded on a multi-electrode array. *B*, PSTH of the example cell, averaged over eight directions. Dashed lines separate the detected spiking phases. Polar plots at the bottom denote the directional tuning of each individual phase. *C*, average PSTH (mean ± SD; *n* = 133 cells from 21 experiments) of all recorded On–Off DSGCs in response to bars moving in the preferred direction (PD; blue) and the null direction (ND; red) (bin size = 10 ms). Horizontal bars above the traces denote bins where one waveform is significantly higher than the other (colour coded by the higher trace; *P* < 0.05). *D*, DSI of distinct response phases detected in all recorded On–Off DSGCs ($P_{\text{On-Del On}}$ = 7.5 × 10^{-19}; $P_{\text{Pre-Del On}}$ = 0.001; $P_{\text{Del On–Off}}$ = 1.3 × 10^{-27}; $P_{\text{On–Off}}$ = 0.07). *E*, histogram of the deviation of the On (top left), delayed-On (top right) and Off (bottom) phases preferred direction from the preferred direction calculated in response to gratings. *F*, same as in *D*, but for the four On–Off DSGC subtypes, determined according to their cardinal preferred direction. One-way ANOVA, *******P* < 0.001 and ********P* < 0.0001. Abbreviations: A, anterior; DSGC, direction-selective ganglion cell; DSI, direction-selective index; FR, firing rate; I, inferior; P, posterior; PSTH, peristimulus time histogram; S, superior.

are almost exclusively tuned to the original preferred direction, the delayed-On phase, despite a slightly higher variability, is tuned primarily to the opposite direction (Fig. 8*E*). This null-tuned delayed-On phase can be found in all subtypes of On–Off DSGCs in response to moving bars (Fig. 8*F*). To ensure that the appearance of the delayed On phase does not depend on the order of polarity presentation, we analysed additional experiments in which moving black bars were presented on a grey background. We found that the null-tuned delayed phase occurred in response to the brighter edge, whether it was the leading edge (as in the case of white bars on a black background) or the trailing edge of the bars (as in the case of black bars on a grey background; Fig. A7*A* and *B*). Finally, we found that a similar delayed phase was present in all the On-DSGC subtypes detected in the MEA recordings (Fig. A6*C*), suggesting that the null-tuned delayed-On phase is a prominent feature of retinal DSGCs and can be found across DSGC types and in various light-adaptation conditions.

Discussion

We show that the receptive fields of pDSGCs expand and that their surround is strengthened following light adaptation. These changes in the receptive field expose the antagonistic nature of their directional response, whereby the centre remains tuned to the original preferred direction and the surround evokes a response in the null direction. The null-tuned response phase originates from an excitatory input in the surround, beyond the dendritic arbor of the cell, on preferred side of pDSGCs. This finding is generalized to other DSGC subtypes, suggesting that the null-tuned response is a fundamental motif in the retinal computation of motion, which is enhanced with light adaptation.

Direction-selective ganglion cells rely on different mechanisms to encode the motion of bars and gratings

Inhibition from SACs underlies the directional responses of DSGCs via two main mechanisms: (i) temporal offset of inhibition and excitation, a result of asymmetric null-side inhibition; and (ii) the centrifugal preference of SAC processes (Ankri et al., 2020; Briggman et al., 2011; Euler et al., 2002; Fransen & Borghuis, 2017; Wei et al., 2011; Yonehara et al., 2011). The recruitment of these mechanisms might depend on the nature of the moving stimulus. Previously, we showed that RVS eliminates the centrifugal preference of SAC processes, which can lead to a reversal of the directional preference of DSGCs in response to moving gratings (Ankri et al., 2020). This reversal depends on inhibition and results from

a surround-mediated temporal shift in the response of SACs that overcomes the anatomical constraints of the null-side inhibition. In the present study, we find that the asymmetric organization of the inhibitory inputs to DSGCs is masked by the strong surround excitation that emerges following light adaptation. The masking of asymmetric null-side inhibition combined with the loss of SAC centrifugal preference uncovers a new mechanism for direction selectivity that relies on excitation. In response to moving bars, excitation tunes the activity in the centre receptive field to the preferred direction, whereas in the surround, excitation supports a null direction computation. Thus, light adaptation reveals a new role for excitation in direction selectivity. Moreover, it demonstrates the presence of at least two mechanisms that are used by the surround receptive field to encode the null direction; one is mediated by inhibition (Ankri et al., 2020) and the other relies on excitation.

Excitatory mechanisms for direction selectivity

Inhibitory inputs to DSGCs are undoubtedly the main drive for retinal direction selectivity. Although directionally tuned excitation to DSGCs was suggested to support the computation (Chen & Wei, 2018; Fried et al., 2005; Lee et al., 2010; Matsumoto et al., 2021; Poleg-Polsky & Diamond, 2016b; Taylor & Vaney, 2002), other studies challenged this claim (Chen et al., 2014; Park et al., 2014; Vaney et al., 2012; Yonehara et al., 2013). Directional excitation was even suggested to be an artefact of an imperfect space clamp and to reflect asymmetric inhibition (Poleg-Polsky & Diamond, 2011). The directional excitation we found in response to moving bars could not be explained by a mere distortion of the recorded inputs coming from asymmetric inhibitory currents. First, before light adaptation, Off excitation but not On excitation shows direction selectivity, although On and Off inhibitory inputs are equally asymmetric. Second, although inhibition becomes symmetric following light adaptation, we find an asymmetric, null-tuned excitatory input on the preferred side of the pDSGC.

A spatially asymmetric glutamatergic input on the preferred side of pDSGCs was recently described and was suggested to support the computation of interrupted motion (Ding et al., 2021). The surround-mediated excitation that we find is tuned to the null direction and could be the result of direction-selective input from bipolar cells, which is mediated by inputs from SACs and wide-field amacrine cells (Matsumoto et al., 2021). Our pharmacology experiments demonstrated that a delayed excitatory phase is masked by GABA inhibition before light adaptation. The fact that gabazine application exposed non-directional surround activity suggests that the increase in the receptive field relies on the expansion of

bipolar cell activation, whereas the directional asymmetry of the response depends on GABAergic inhibition. Glycinergic cells were previously suggested to underlie the experience-dependent modulation of glutamate from bipolar cells to pDSGCs (Huang et al., 2022). The abolishment of the surround excitation by strychnine suggests that a delicate balance between inhibitory inputs underlies this null-tuned response phase.

Contribution of On and Off pathways to the light adaptation shifts in pDSGCs

On–Off pDSGCs receive inputs from both the On and Off pathways, and classically, their On and Off directional responses are thought to be mediated by independent channels (Famiglietti & Kolb, 1976; Nelson et al., 1978; Schiller, 1992). Yet, the On and Off pathways can be intermingled and do not always act as two independent streams of information. Upstream to pDSGCs, horizontal cells can serve as a hub for sign-inverting bipolar cell inputs (Szikra et al., 2014), and cross-over between the two pathways can also arise through amacrine cells via disinhibition (Demb & Singer, 2012; Taylor & Smith, 2011; Werblin, 2010). Downstream, On and Off dendrites of pDSGCs are connected via multiple thin dendritic branches (Huang et al., 2022; Rivlin-Etzion et al., 2011). Our results portray several differences in On- and Off-inputs to pDSGCs, some of which occur following light adaptation. First, before light adaptation the Off response is stronger, or at least equal to the On response, and following light adaptation the On phase dominates the response. Second, the spatial asymmetry of the On receptive field is very prominent following light adaptation, whereas the Off receptive field seems to be somewhat more symmetric (Fig. 1). Third, prior to light adaptation, excitation seems to contribute to the mechanisms for direction selectivity in the Off response, but not in the On response, whereas following light adaptation, the On response seems to rely strongly on directional excitation (Fig. 6). Although the On-delayed null-tuned response could arise via surround activation of the Off pathway, blocking the On pathway using L-AP4 eliminated most of the RVS-mediated On response (Fig. A5). The remaining response probably originated from the Off pathway, but it was not prominent enough to be considered as the main contributor to the surround-mediated null-tuned response.

Temporal coding and multidimensional information transfer

In a recent work, a second receptive field outside the classical receptive field was described in neurons of the visual cortex, and the two receptive fields were mutually antagonistic (Keller et al., 2020). The temporal characteristics of the surround-mediated cortical response were surprisingly similar to the null-direction response of retinal DSGCs, exhibiting a prolonged activity in comparison to the centre responses. Apart from spatial changes in the receptive field organization of pDSGCs, light adaptation led to shifted kinetics, and the overall response became more sustained. This was in response to both bar stimulation and static spots (Fig. 1; Rivlin-Etzion et al., 2012). This shift might originate presynaptically to pDSGCs, because similar slower kinetics were found in bipolar cells when their response is mediated by the surround (Franke et al., 2017; Strauss et al., 2022). Considering the resemblance of the null-tuned responses we describe here to the cortical equivalent surround-mediated response in terms of temporal characteristics, we suggest that this could be a feature of surround activation and could serve the target structure as a way to discriminate centre from surround responses. Thus, the distinct temporal features add to the opposite directional preferences in the centre and surround receptive fields, and together they might serve to increase the perceptual spatial acuity of motion discrimination in the visual field, using motifs that resemble those used for edge and colour detection.

Flexibility in the polarity and directional tunings of pDSGCs following light adaptation

Although the polarity preferences of retinal ganglion cells can present some flexibility and change with the extent of the visual stimulus and the presented light levels (Kim et al., 2008; Pearson & Kerschensteiner, 2015; Tikidji-Hamburyan et al., 2015), the directional preference of DSGCs is classically considered fixed and hard wired (Chen & Wei, 2018; Ding et al., 2021; Yao et al., 2018). Two previous reports support this notion, showing that the preferred direction of DSGCs remains stable across light levels (Pearson & Kerschensteiner, 2015), and some DSGCs even sharpen their tunings as the stimulus intensity increases (Yao et al., 2018). Nevertheless, our findings that, following light adaptation, DSGCs broaden their directional preference in response to moving bars and can even reverse their preferred direction in response to moving gratings (Ankri et al., 2020; Rivlin-Etzion et al., 2012) suggest that the protocols of light adaptation we used, in which the retina is exposed to photopic light levels, have different implications for the retinal circuitry than those caused by a simple gradual increase in ambient light levels. Notably, our data demonstrate a simultaneous shift in both the polarity preference and the directional response of DSGCs, which seem to arise from a mutual origin, the strengthening of the surround. When dominated by the centre, the Off response of

DSGCs is stronger, and when dominated by the surround, the On response takes over. This suggests that the On and Off circuits have different roles in On–Off DSGCs, hinting that they are not merely mirror symmetric. The simultaneous emergence of the two is shown by the correlation between the On–Off index and the DSI (Fig. 2). Considering the grand fluidity in the function of DSGCs, our findings might have implications for the general approach of identifying DSGCs by their light responses, because light adaptation alters their directional tunings and elicits an oppositely tuned response phase. This light-induced fluidity poses a challenge to the conventional functional identification of retinal ganglion cells.

Appendix
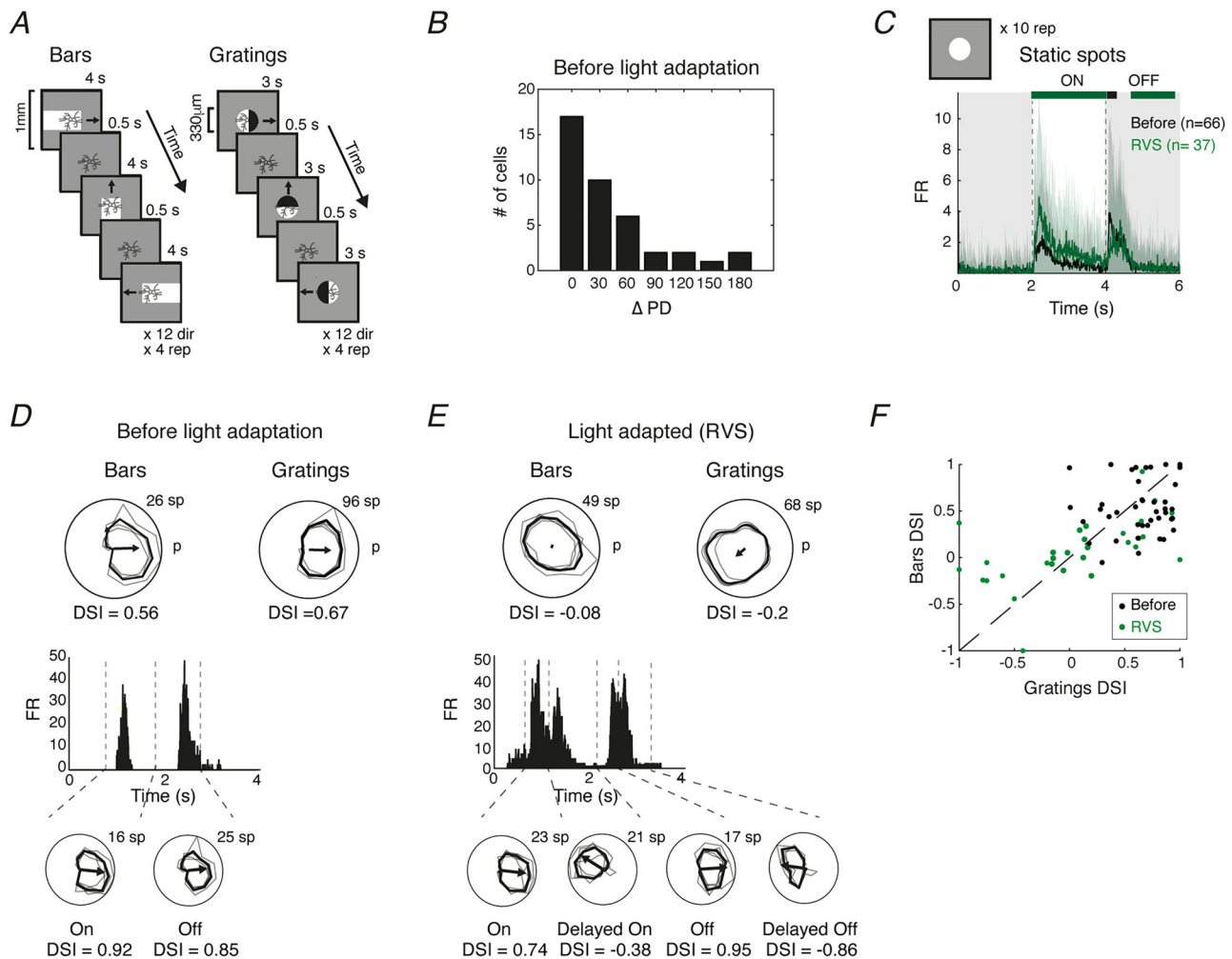
Figure A1. Directional response of posterior-preferring direction-selective ganglion cells to gratings and bars following repetitive visual stimulation
A, illustration of the stimuli used to measure direction selectivity in DSGCs. *B*, histogram of the difference between the preferred direction calculated in the response of pDSGCs to moving gratings and bars before light adaptation ($n = 40$). *C*, PSTH (mean ± SD) of all cells recorded in response to centred static spots (50 µm radius) before and after RVS. The time window of presentation of spots is shown in white. Coloured bars above traces denote the bins where one waveform is significantly higher than the other for On and for Off responses (colour coded by the higher waveform; $P < 0.05$). The number of cells in each condition is in parentheses. *D* and *E*, polar plot and PSTH of example cells recorded in response to bars and gratings before (*D*) and after (*E*) light adaptation with RVS. The PSTH is summed across directions. Separation into spiking phases detected in response to bars is denoted by dashed lines on the PSTHs, and corresponding polar plots are depicted below. *F*, the DSIs calculated in response to bars *vs.* gratings in pDSGCs, before (black; $n = 41$) and after (green; $n = 31$) light adaptation with RVS. Abbreviations: DSGC, direction-selective ganglion cell; DSI, direction-selective index; FR, firing rate; p, posterior; PD, preferred direction; pDSGC, posterior-preferring direction-selective ganglion cell; PSTH, peristimulus time histogram; RVS, repetitive visual stimulation; sp, spikes.
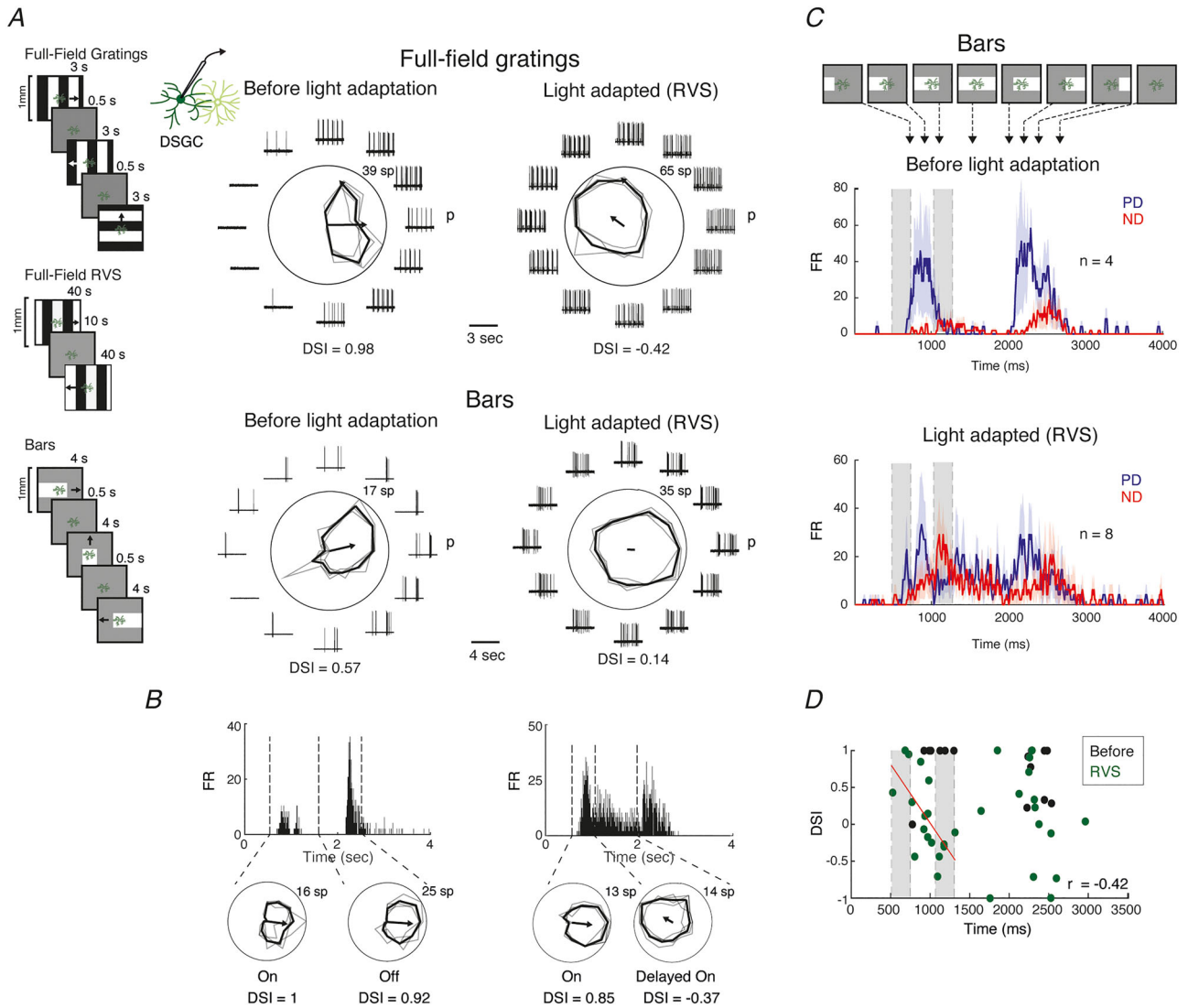
Figure A2. Repetitive visual stimulation-mediated delayed-On phase in response of posterior-preferring direction-selective ganglion cells to moving bars appears at any photopic light adaptation and independent of the spatial extent of adaptation

A, left, schematic diagram of the visual stimuli presented at lower light intensity (5.2×10^3 R*/rod/s); right, loose-patch recordings from an example pDSGC. Polar plots represent the directional tuning in response to full-field gratings (top) and bars (bottom) before (left) and after (right) light adaptation with full-field RVS projected to the cells through the ×20 objective, covering an area of ~1 mm. Black bold line represents the mean; thin lines denote single repetitions. *B*, PSTH of the example cell in *A* in response to a moving bar (top; 10 ms bin), averaged over all directions. Horizontal dashed lines denote different response phases, and polar plots (bottom) show the tuning of each response phase. *C*, PSTHs (mean ± SD) in response to bars moving in the preferred direction (PD; blue) and the null direction (ND; red) before (top) and after (bottom) light adaptation with full-field RVS. The location of the bar at several time points is illustrated at the top. The number of recorded cells in each condition is denoted next to the waveforms. *D*, DSI of distinct phases in pDSGC PSTHs before and after full-field RVS, for all recorded cells, plotted *vs.* time of response peak. Red line denotes the correlation between the DSI and the time of response peak following RVS. Vertical dashed boxes denote the time when the bars hit the estimated surround receptive field, as illustrated in *C*. Abbreviations: DSI, direction-selective index; FR, firing rate; ND, null direction; p, posterior; PD, preferred direction; pDSGC, posterior-preferring direction-selective ganglion cell; PSTH, peristimulus time histogram; RVS, repetitive visual stimulation; sp, spikes.
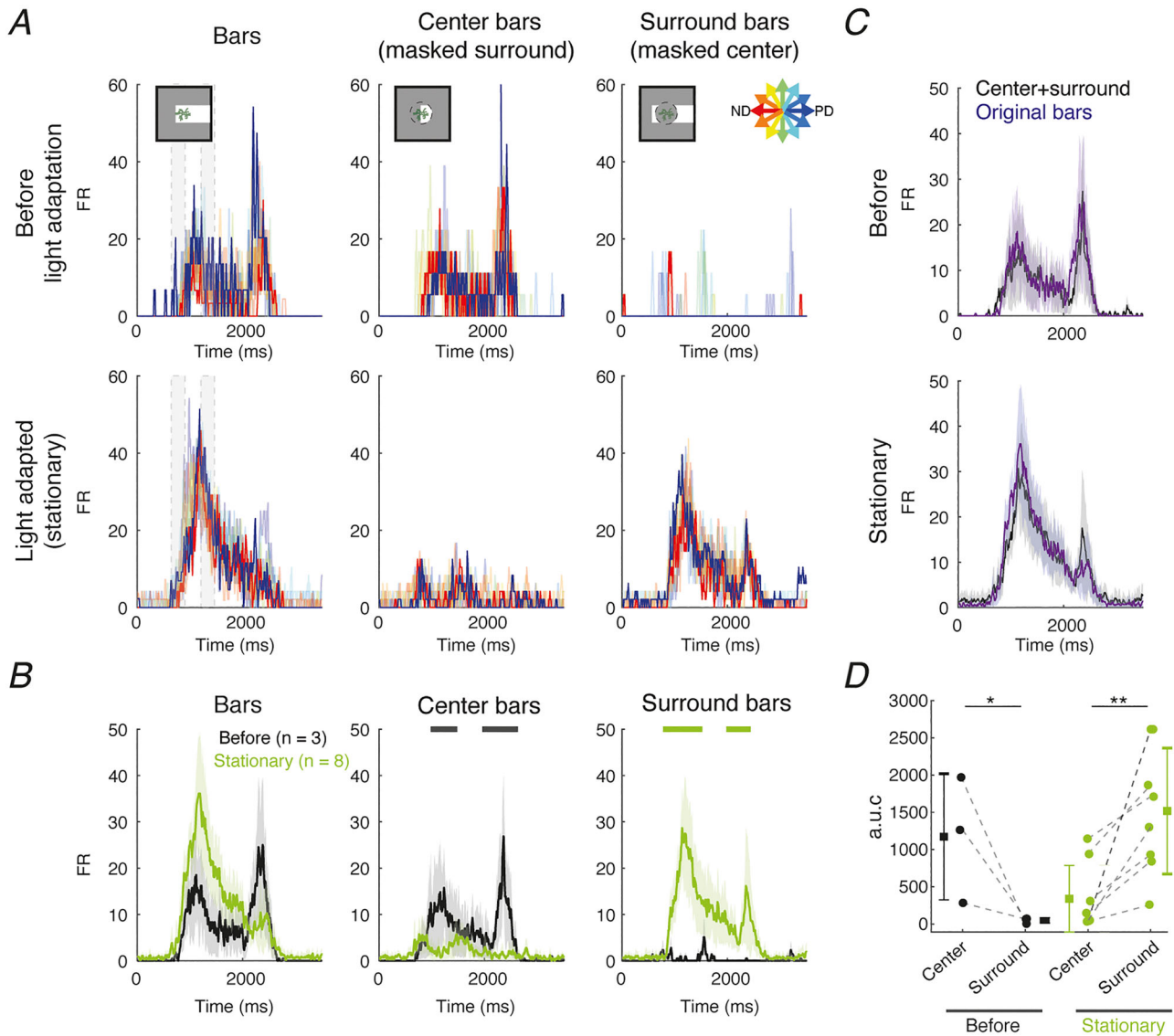
Figure A3. Light adaptation enhances the contribution of the surround receptive field to the response of posterior-preferring direction-selective ganglion cells and decreases the contribution of the centre
A, directions mean PSTH (colour coded in the inset) of all cells before (top) and after (bottom) light adaptation with stationary illumination, in response to three bar presentations: full-field bars (left), bars with a mask in the surround ('centre bars', middle) and bars with a mask in the centre receptive field ('surround bars', right). Visual stimuli are illustrated above. *B*, PSTH (mean ± SD) of the population in *A*, averaged across directions, before (black) and after (green) light adaptation. The number of cells in each condition is in parentheses. Coloured bars above traces denote the time windows when one waveform is significantly higher than the other ($P < 0.05$). *C*, PSTH (mean ± SD) in response to full-field bars (purple) overlaid with the summation of the PSTH in response to surround masking and centre masking (black). Summation of the centre and surround waveforms while masking specific portions of the receptive field produced waveforms that resemble the unmasked response. The waveforms recapitulated the shift in the On–Off dominance of the response following light adaptation. *D*, summation of the area under the curve (a.u.c) in the PSTH response to centre (surround masking) and to surround (centre masking), before and after light adaptation ($P_{\text{before}} = 0.05$; $P_{\text{stationary}} = 0.006$). The mean ± SD are shown. Student's paired *t* test, *P < 0.05 and **P < 0.01. Abbreviations: FR, firing rate; ND, null direction; PD, preferred direction; PSTH, peristimulus time histogram.
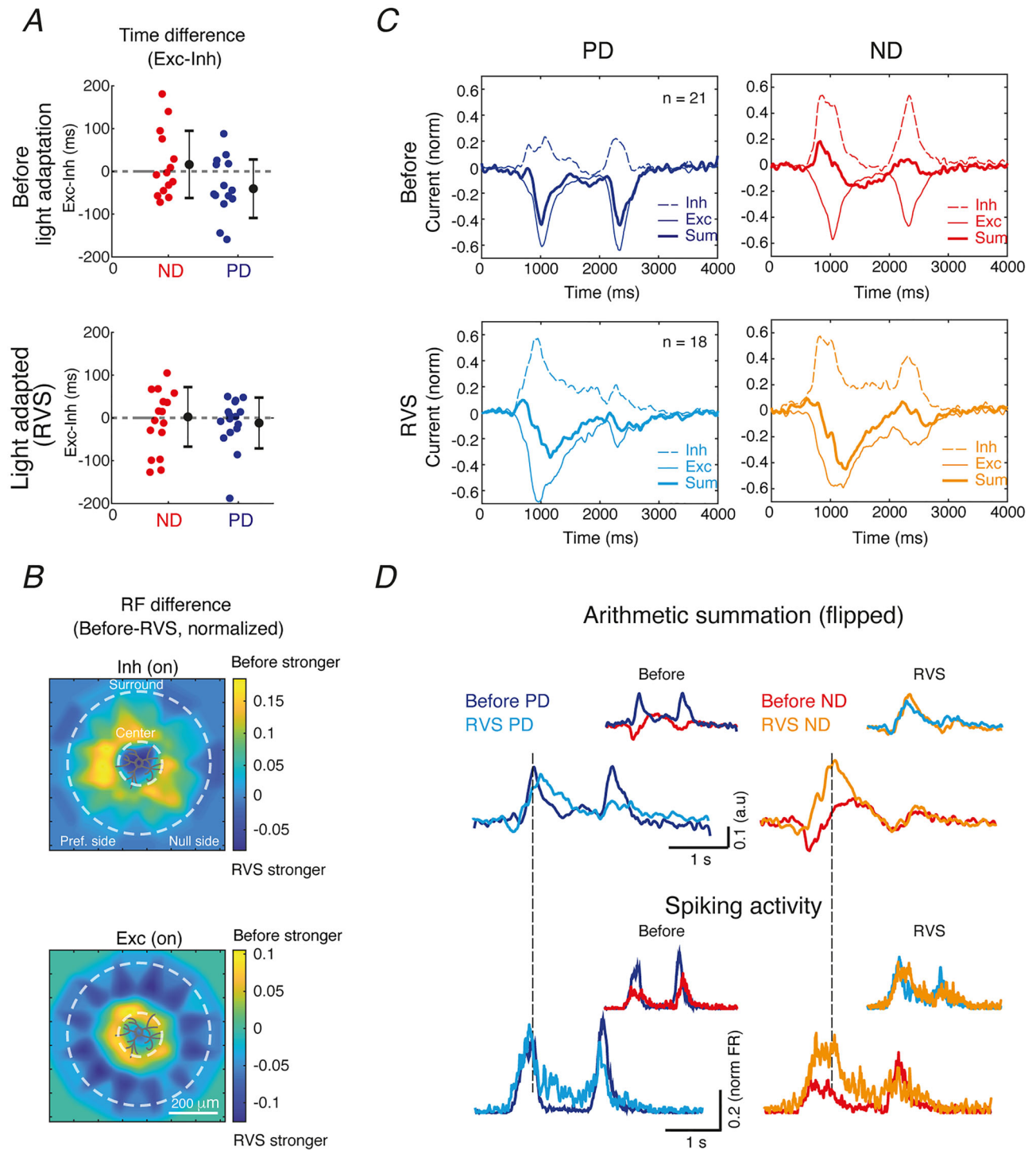
Figure A4. The effect of repetitive visual stimulation on inhibitory and excitatory inputs to posterior-preferring direction-selective ganglion cells

A, the difference between the response onset of inhibition and excitation (see Methods), for a bar moving in null and preferred directions, before (top; ND On: 16.3 ± 78.5; and PD On: −35.6 ± 68.4; mean ± SD) and after light adaptation with RVS (bottom; ND On: 2.7 ± 69.5; and PD On: −11.9 ± 59.5; mean ± SD). *B*, pDSGC On receptive fields following RVS subtracted from the On fields calculated before light adaptation for inhibition (top) and excitation (bottom). The resulting difference is colour coded on the right. Estimated centre and surround areas are illustrated by dashed circles. *C*, normalized average inhibitory and excitatory inputs, in response to bars

moving in the preferred direction (PD; blue, cyan; left) and the null direction (ND; red, orange; right), before (top) and after RVS (bottom). Bold traces are waveforms produced by the arithmetic summation ('sum') of excitatory and inhibitory normalized currents. *D*, comparison of summation of inputs (top, flipped upside-down) and spiking activity of pDSGCs (bottom, mean peristimulus time histogram; 10 ms bin) in response to motion in the preferred direction (PD; blue, cyan) and the null direction (ND; red, orange). Abbreviations: Exc, excitation; FR, firing rate; Inh, inhibition; ND, null direction; PD, preferred direction; pDSGC, posterior-preferring direction-selective ganglion cell; RVS, repetitive visual stimulation.
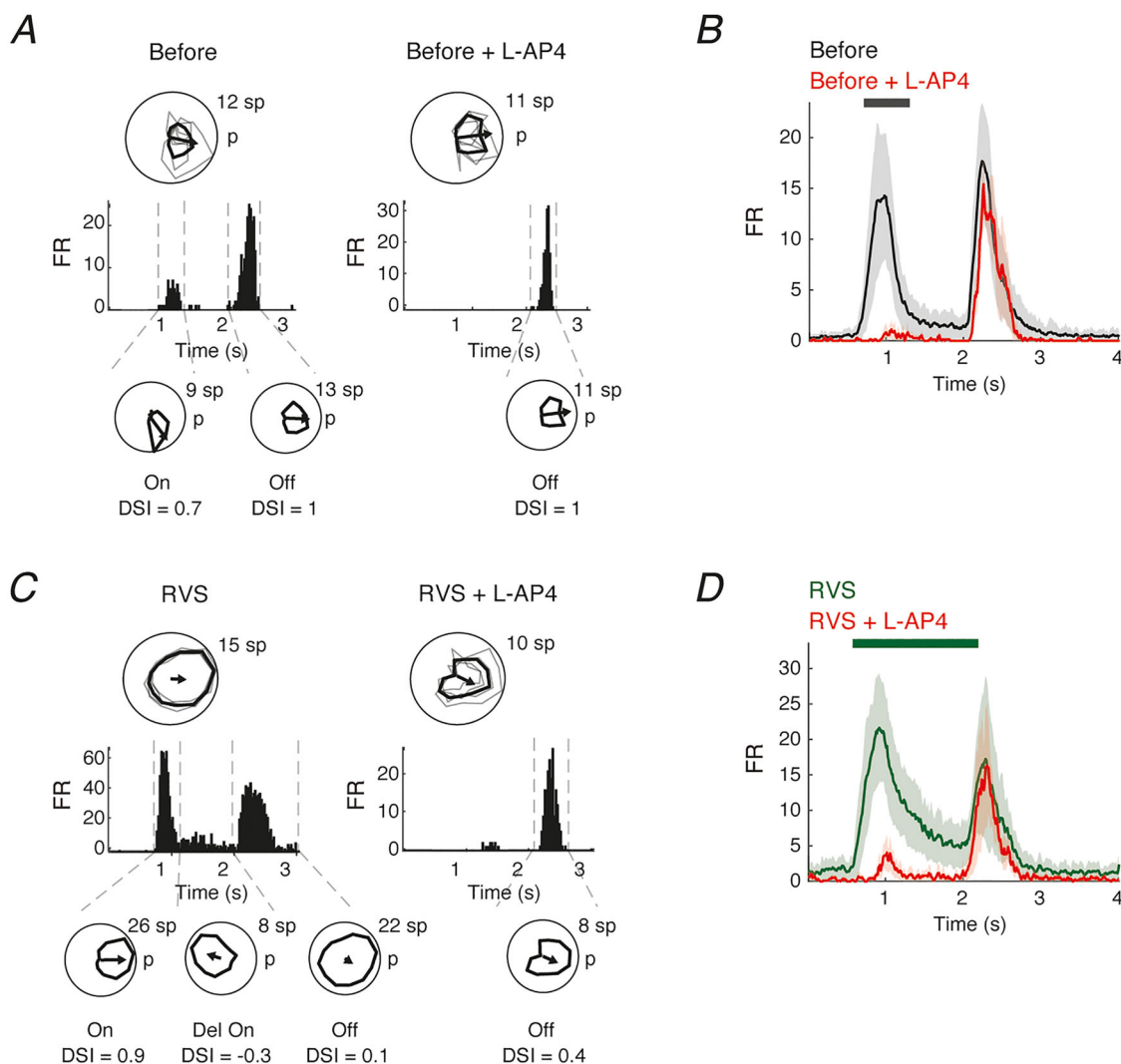

Figure A5. The delayed-On phase is mostly mediated by the On pathway
A, PSTH from an example pDSGC before light adaptation, prior to (left) and following (right) L-AP4 application, recorded in patch-clamp mode. Polar plots of the total response are shown on top of the PSTH (sum of all directions). Dashed vertical lines denote the detected phases; polar plots of individual phases are plotted below the PSTH. *B*, population average PSTH of pDSGCs recorded before (black) and after L-AP4 application (red; *n* = 5). Horizontal bars above the trace mark the area where one of the waveforms is significantly higher than the other ($P < 0.05$). *C*, as in *A*, but for an example pDSGC following RVS. *D*, same as *B*, but for RVS-adapted pDSGCs (*n* = 6). Abbreviations: DSI, direction-selective index; FR, firing rate; L-AP4, L-2-amino-4-phosphonobutyric acid; pDSGC, posterior-preferring direction-selective ganglion cell; PSTH, peristimulus time histogram; RVS, repetitive visual stimulation; sp, spikes.
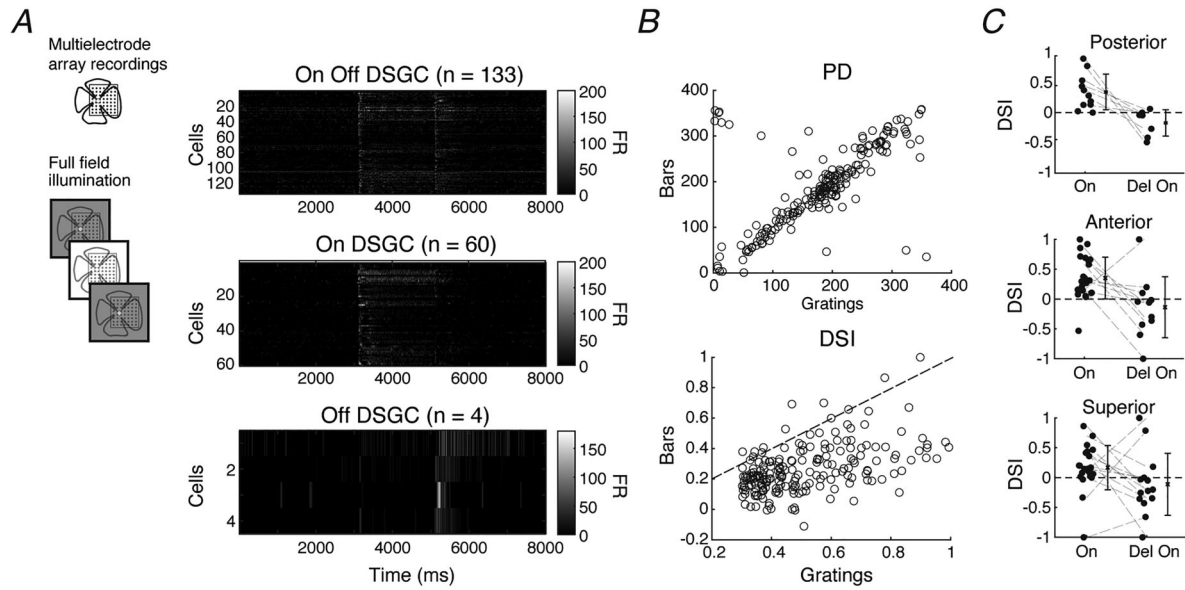
Figure A6. A delayed-On component is a prominent feature in all On-direction-selective ganglion cell subtypes

A, DSGC responses recorded by multi-electrode array to full-field light stimulation (illustrated on the left; light onset starts at 3000 ms and ends at 5000 ms) used to determine the polarity of the cell. Each line represents the mean activity (firing rate) of one DSGC. The DSGCs were defined as On–Off, On and Off DSGCs accordingly. The number of cells in each group is mentioned in parentheses. *B*, top, the preferred direction of On–Off DSGCs in response to moving bars plotted against their preferred direction in response to drifting gratings; bottom, the DSI calculated from the response of On–Off DSGCs to bars plotted against their DSI in response to gratings. The response to bars and gratings was tuned to the same PD, although the DSI was lower in response to bars. This can be explained by the null-tuned delayed-On phase that occurs in response to bars. *C*, the DSI of identified response phases in On DSGCs. On cells displayed a delayed spiking phase that is either untuned or tuned to the ND. Abbreviations: DSGC, direction-selective ganglion cell; DSI, direction-selective index; ND, null direction; PD, preferred direction.
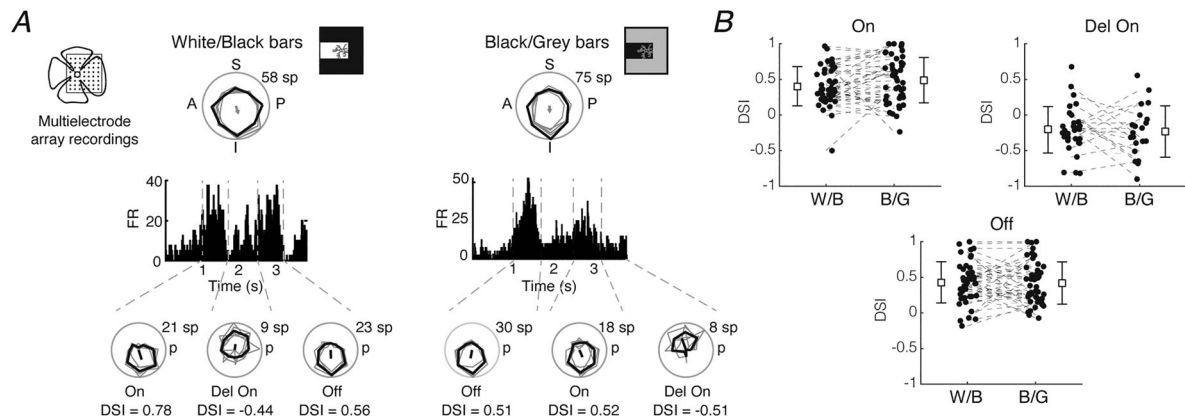

Figure A7. The emergence of the null-tuned delayed On phase does not depend on the polarity of the bar

A, top, polar plot and PSTH from an example cell recorded in a multi-electrode array, presented with white bars moving on a black background (white/black bars; left) and with black bars on a grey background (black/grey bars; right); bottom, polar plots of the different phases. Cut-offs between phases are marked by dashed grey lines above the PSTH. The DSI of each phase is denoted below the polar plots. *B*, the DSI of the different phases from all DSGCs recorded in a multi-electrode array, in response to white on black bars (W/B) and black on grey bars (B/G) ($n = 44$ cells in six experiments). Values from the same cells are connected by dashed lines. The mean ± SD are plotted next to the values. On-delayed phases were tuned to the opposite direction whether they were evoked by the leading or trailing edges of the bars. There was no significant difference between any of the response phases ($P_{On} = 0.21$; $P_{Del-on} = 0.81$; $P_{Off} = 0.86$; Student's paired *t* test). Abbreviations: A, anterior; DSGC, direction-selective ganglion cell; DSI, direction-selective index; FR, firing rate; I, inferior; P, posterior; PSTH, peristimulus time histogram; S, superior; sp, spikes.

References

Ankri, L., Ezra-Tsur, E., Maimon, S. R., Kaushansky, N., & Rivlin-Etzion, M. (2020). Antagonistic center-surround mechanisms for direction selectivity in the retina. *Cell Reports*, **31**(5), 107608.

Barlow, H. B., Fitzhugh, R., & Kuffler, S. W. (1957). Change of organization in the receptive fields of the cat's retina during dark adaptation. *The Journal of Physiology*, **137**(3), 338–354.

Briggman, K. L., Helmstaedter, M., & Denk, W. (2011). Wiring specificity in the direction-selectivity circuit of the retina. *Nature*, **471**(7337), 183–188.

Brombas, A., Kalita-de Croft, S., Cooper-Williams, E. J., & Williams, S. R. (2017). Dendro-dendritic cholinergic excitation controls dendritic spike initiation in retinal ganglion cells. *Nature Communications*, **8**, 15683.

Chaffiol, A., Ishii, M., Cao, Y., & Mangel, S. C. (2017). Dopamine regulation of GABAA receptors contributes to light/dark modulation of the ON-cone bipolar cell receptive field surround in the retina. *Current Biology*, **27**(17), 2600–2609.e4.

Chávez, A. E., Grimes, W. N., & Diamond, J. S. (2010). Mechanisms underlying lateral GABAergic feedback onto rod bipolar cells in rat retina. *The Journal of Neuroscience*, **30**(6), 2330–2339.

Chen, M., Lee, S., Park, S. J. H., Looger, L. L., & Zhou, Z. J. (2014). Receptive field properties of bipolar cell axon terminals in direction-selective sublaminas of the mouse retina. *Journal of Neurophysiology*, **112**(8), 1950–1962.

Chen, Q., Pei, Z., Koren, D., & Wei, W. (2016). Stimulus-dependent recruitment of lateral inhibition underlies retinal direction selectivity. *eLife*, **5**, e21053.

Chen, Q., & Wei, W. (2018). Stimulus-dependent engagement of neural mechanisms for reliable motion detection in the mouse retina. *Journal of Neurophysiology*, **120**(3), 1153–1161.

Cicerone, C. M., Green, D. G., & Tong, L. (1979). Sites of light and dark adaptation in rat retina. *Vision Research*, **19**(4), 358.

Cowan, C. S., Sabharwal, J., Seilheimer, R. L., & Wu, S. M. (2017). Distinct subcomponents of mouse retinal ganglion cell receptive fields are differentially altered by light adaptation. *Vision Research*, **131**, 96–105.

Dedek, K., Pandarinath, C., Alam, N. M., Wellershaus, K., Schubert, T., Willecke, K., Prusky, G. T., Weiler, R., & Nirenberg, S. (2008). Ganglion cell adaptability: Does the coupling of horizontal cells play a role? *PLoS ONE*, **3**(3), e1714.

Demb, J. B. (2008). Functional circuitry of visual adaptation in the retina. *The Journal of Physiology*, **586**(18), 4377–4384.

Demb, J. B., & Singer, J. H. (2012). Intrinsic properties and functional circuitry of the AII amacrine cell. *Visual Neuroscience*, **29**(1), 51–60.

Derrington, A. M., & Lennie, P. (1982). The influence of temporal frequency and adaptation level on receptive field organization of retinal ganglion cells in cat. *The Journal of Physiology*, **333**, 343–366.

Ding, J., Chen, A., Chung, J., Acaron Ledesma, H., Wu, M., Berson, D. M., Palmer, S. E., & Wei, W. (2021). Spatially displaced excitation contributes to the encoding of inter-rupted motion by a retinal direction-selective circuit. *eLife*, **10**, e68181.

Enroth-Cugell, C., & Pinto, L. H. (1972). Properties of the surround response mechanism of cat retinal ganglion cells and centre-surround interaction. *The Journal of Physiology*, **220**(2), 403–439.

Euler, T., Detwiler, P. B., & Denk, W. (2002). Directionally selective calcium signals in dendrites of starburst amacrine cells. *Nature*, **418**(6900), 845–852.

Fahey, P. K., & Burkhardt, D. A. (2003). Center-surround organization in bipolar cells: Symmetry for opposing contrasts. *Visual Neuroscience*, **20**(1), 1–10.

Famiglietti, E. V., & Kolb, H. (1976). Structural basis for ON-and OFF-center responses in retinal ganglion cells. *Science*, **194**(4261), 193–195.

Farrow, K., Teixeira, M., Szikra, T., Viney, T. J., Balint, K., Yonehara, K., & Roska, B. (2013). Ambient illumination toggles a neuronal circuit switch in the retina and visual perception at cone threshold. *Neuron*, **78**(2), 325–338.

Franke, K., Berens, P., Schubert, T., Bethge, M., Euler, T., & Baden, T. (2017). Inhibition decorrelates visual feature representations in the inner retina. *Nature*, **542**(7642), 439–444.

Fransen, J. W., & Borghuis, B. G. (2017). Temporally diverse excitation generates direction-selective responses in ON-and OFF-type retinal starburst amacrine cells. *Cell Reports*, **18**(6), 1356–1365.

Fried, S. I., Münch, T. A., & Werblin, F. S. (2005). Directional selectivity is formed at multiple levels by laterally offset inhibition in the rabbit retina. *Neuron*, **46**(1), 117–127.

Fried, S. I., Münch, T. A., & Werblin, F. S. (2002). Mechanisms and circuitry underlying directional selectivity in the retina. *Nature*, **420**(6914), 411–414.

Hanson, L., Sethuramanujam, S., deRosenroll, G., Jain, V., & Awatramani, G. B. (2019). Retinal direction selectivity in the absence of asymmetric starburst amacrine cell responses. *eLife*, **8**, e42392.

Huang, X., Kim, A. J., Acarón Ledesma, H., Ding, J., Smith, R. G., & Wei, W. (2022). Visual stimulation induces distinct forms of sensitization of on-off direction-selective ganglion cell responses in the dorsal and ventral retina. *The Journal of Neuroscience*, **42**(22), 4449–4469.

Huberman, A. D., Wei, W., Elstrott, J., Stafford, B. K., Feller, M. B., & Barres, B. A. (2009). Genetic identification of an On-Off direction-selective retinal ganglion cell subtype reveals a layer-specific subcortical map of posterior motion. *Neuron*, **62**(3), 327–334.

Keller, A. J., Roth, M. M., & Scanziani, M. (2020). Feedback generates a second receptive field in neurons of the visual cortex. *Nature*, **582**(7813), 545–549.

Kim, I.-J., Zhang, Y., Yamagata, M., Meister, M., & Sanes, J. R. (2008). Molecular identification of a retinal cell type that responds to upward motion. *Nature*, **452**(7186), 478–482.

Kuffler, S. W. (1953). Discharge patterns and functional organization of mammalian retina. *Journal of Neurophysiology*, **16**(1), 37–68.

Lee, S., Kim, K., & Zhou, Z. J. (2010). Role of ACh-GABA cotransmission in detecting image motion and motion direction. *Neuron*, **68**(6), 1159–1172.

Marr, D., & Hildreth, E. (1980). Theory of edge detection. *Proceedings of the Royal Society of London Series B, Containing Papers of A Biological Character Royal Society (Great Britain)*, **207**(1167), 187–217.

Matsumoto, A., Agbariah, W., Nolte, S. S., Andrawos, R., Levi, H., Sabbah, S., & Yonehara, K. (2021). Direction selectivity in retinal bipolar cell axon terminals. *Neuron*, **109**(18), 2928–2942.e8.

Nath, A., Grimes, W. N., & Diamond, J. S. (2023). Layers of inhibitory networks shape receptive field properties of AII amacrine cells. *Cell Reports*, **42**(11), 113390.

Nelson, R., Famiglietti, E. V., & Kolb, H. (1978). Intracellular staining reveals different levels of stratification for on- and off-center ganglion cells in cat retina. *Journal of Neurophysiology*, **41**(2), 472–483.

Oyster, C. W., & Barlow, H. B. (1967). Direction-selective units in rabbit retina: Distribution of preferred directions. *Science*, **155**(3764), 841–842.

Pachitariu, M., Steinmetz, N., Kadir, S., Carandini, M., & Harris, K. D. (2016). Kilosort: Realtime spike-sorting for extracellular electrophysiology with hundreds of channels. *BioRxiv*.

Park, S. J. H., Kim, I.-J., Looger, L. L., Demb, J. B., & Borghuis, B. G. (2014). Excitatory synaptic inputs to mouse on-off direction-selective retinal ganglion cells lack direction tuning. *The Journal of Neuroscience*, **34**(11), 3976–3981.

Pearson, J. T., & Kerschensteiner, D. (2015). Ambient illumination switches contrast preference of specific retinal processing streams. *Journal of Neurophysiology*, **114**(1), 540–550.

Pei, Z., Chen, Q., Koren, D., Giammarinaro, B., Acaron Ledesma, H., & Wei, W. (2015). Conditional knock-out of vesicular GABA transporter gene from starburst amacrine cells reveals the contributions of multiple synaptic mechanisms underlying direction selectivity in the retina. *The Journal of Neuroscience*, **35**(38), 13219–13232.

Poleg-Polsky, A., & Diamond, J. S. (2011). Imperfect space clamp permits electrotonic interactions between inhibitory and excitatory synaptic conductances, distorting voltage clamp recordings. *PLoS ONE*, **6**(4), e19463.

Poleg-Polsky, A., & Diamond, J. S. (2016a). NMDA receptors multiplicatively scale visual signals and enhance directional motion discrimination in retinal ganglion cells. *Neuron*, **89**(6), 1277–1290.

Poleg-Polsky, A., & Diamond, J. S. (2016b). Retinal circuitry balances contrast tuning of excitation and inhibition to enable reliable computation of direction selectivity. *The Journal of Neuroscience*, **36**(21), 5861–5876.

Rieke, F., & Rudd, M. E. (2009). The challenges natural images pose for visual adaptation. *Neuron*, **64**(5), 605–616.

Rivlin-Etzion, M., Grimes, W. N., & Rieke, F. (2018). Flexible neural hardware supports dynamic computations in retina. *Trends in Neurosciences*, **41**(4), 224–237.

Rivlin-Etzion, M., Wei, W., & Feller, M. B. (2012). Visual stimulation reverses the directional preference of direction-selective retinal ganglion cells. *Neuron*, **76**(3), 518–525.

Rivlin-Etzion, M., Zhou, K., Wei, W., Elstrott, J., Nguyen, P. L., Barres, B. A., Huberman, A. D., & Feller, M. B. (2011). Transgenic mice reveal unexpected diversity of on-off direction-selective retinal ganglion cell subtypes and brain structures involved in motion processing. *The Journal of Neuroscience*, **31**(24), 8760–8769.

Roska, B., Nemeth, E., Orzo, L., & Werblin, F. S. (2000). Three levels of lateral inhibition: A space-time study of the retina of the tiger salamander. *The Journal of Neuroscience*, **20**(5), 1941–1951.

Rossant, C., & Harris, K. D. (2013). Hardware-accelerated interactive data visualization for neuroscience in Python. *Frontiers in Neuroinformatics*, **7**, 36.

Rossant, C., Kadir, S. N., Goodman, D. F. M., Schulman, J., Hunter, M. L. D., Saleem, A. B., Grosmark, A., Belluscio, M., Denfield, G. H., Ecker, A. S., Tolias, A. S., Solomon, S., Buzsaki, G., Carandini, M., & Harris, K. D. (2016). Spike sorting for large, dense electrode arrays. *Nature Neuroscience*, **19**(4), 634–641.

Sabbah, S., Gemmer, J. A., Bhatia-Lin, A., Manoff, G., Castro, G., Siegel, J. K., Jeffery, N., & Berson, D. M. (2017). A retinal code for motion along the gravitational and body axes. *Nature*, **546**(7659), 492–497.

Sagdullaev, B. T., & McCall, M. A. (2005). Stimulus size and intensity alter fundamental receptive-field properties of mouse retinal ganglion cells in vivo. *Visual Neuroscience*, **22**(5), 649–659.

Schiller, P. H. (1992). The ON and OFF channels of the visual system. *Trends in Neurosciences*, **15**(3), 86–92.

Segev, R., Goodhouse, J., Puchalla, J., & Berry, M. J. (2004). Recording spikes from a large fraction of the ganglion cells in a retinal patch. *Nature Neuroscience*, **7**(10), 1154–1161.

Sethuramanujam, S., McLaughlin, A. J., deRosenroll, G., Hoggarth, A., Schwab, D. J., & Awatramani, G. B. (2016). A central role for mixed acetylcholine/gaba transmission in direction coding in the retina. *Neuron*, **90**(6), 1243–1256.

Strauss, S., Korympidou, M. M., Ran, Y., Franke, K., Schubert, T., Baden, T., Berens, P., Euler, T., & Vlasits, A. L. (2022). Center-surround interactions underlie bipolar cell motion sensitivity in the mouse retina. *Nature Communications*, **13**(1), 5574.

Szikra, T., Trenholm, S., Drinnenberg, A., Jüttner, J., Raics, Z., Farrow, K., Biel, M., Awatramani, G., Clark, D. A., Sahel, J. A., da Silveira, R. A., & Roska, B. (2014). Rods in daylight act as relay cells for cone-driven horizontal cell-mediated surround inhibition. *Nature Neuroscience*, **17**(12), 1728–1735.

Taylor, W. R., & Smith, R. G. (2011). Trigger features and excitation in the retina. *Current Opinion in Neurobiology*, **21**(5), 672–678.

Taylor, W. R., & Vaney, D. I. (2002). Diverse synaptic mechanisms generate direction selectivity in the rabbit retina. *The Journal of Neuroscience*, **22**(17), 7712–7720.

Tikidji-Hamburyan, A., Reinhard, K., Seitter, H., Hovhannisyan, A., Procyk, C. A., Allen, A. E., Schenk, M., Lucas, R. J., & Münch, T. A. (2015). Retinal output changes qualitatively with every change in ambient illuminance. *Nature Neuroscience*, **18**(1), 66–74.

Trenholm, S., Johnson, K., Li, X., Smith, R. G., & Awatramani, G. B. (2011). Parallel mechanisms encode direction in the retina. *Neuron*, **71**(4), 683–694.

Vaney, D. I., Sivyer, B., & Taylor, W. R. (2012). Direction selectivity in the retina: Symmetry and asymmetry in structure and function. *Nature Reviews Neuroscience*, **13**(3), 194–208.

Vlasits, A. L., Bos, R., Morrie, R. D., Fortuny, C., Flannery, J. G., Feller, M. B., & Rivlin-Etzion, M. (2014). Visual stimulation switches the polarity of excitatory input to starburst amacrine cells. *Neuron*, **83**(5), 1172–1184.

Warwick, R. A., Heukamp, A. S., Riccitelli, S., & Rivlin-Etzion, M. (2023). Dopamine differentially affects retinal circuits to shape the retinal code. *The Journal of Physiology*, **601**(7), 1265–1286.

Warwick, R. A., Kaushansky, N., Sarid, N., Golan, A., & Rivlin-Etzion, M. (2018). Inhomogeneous encoding of the visual field in the mouse retina. *Current Biology*, **28**(5), 655–665.e3.

Warwick, R. A., Riccitelli, S., Heukamp, A. S., Yaakov, H., Ankri, L., Mayzel, J., Gilead, N., Parness-Yossifon, R., Di Marco S. & Rivlin-Etzion, M. (2024). Top-down modulation of the retinal code via histaminergic neurons of the hypo-thalamus. *Science Advances*, **10**(35), eadk4062.

Wei, W., Hamby, A. M., Zhou, K., & Feller, M. B. (2011). Development of asymmetric inhibition underlying direction selectivity in the retina. *Nature*, **469**(7330), 402–406.

Werblin, F. S. (2010). Six different roles for crossover inhibition in the retina: Correcting the nonlinearities of synaptic transmission. *Visual Neuroscience*, **27**(1–2), 1–8.

Wienbar, S., & Schwartz, G. W. (2018). The dynamic receptive fields of retinal ganglion cells. *Progress in Retinal and Eye Research*, **67**, 102–117.

Yao, X., Cafaro, J., McLaughlin, A. J., Postma, F. R., Paul, D. L., Awatramani, G., & Field, G. D. (2018). Gap junctions contribute to differential light adaptation across direction-selective retinal ganglion cells. *Neuron*, **100**(1), 216–228.e6.

Yonehara, K., Balint, K., Noda, M., Nagel, G., Bamberg, E., & Roska, B. (2011). Spatially asymmetric reorganization of inhibition establishes a motion-sensitive circuit. *Nature*, **469**(7330), 407–410.

Yonehara, K., Farrow, K., Ghanem, A., Hillier, D., Balint, K., Teixeira, M., Jüttner, J., Noda, M., Neve, R. L., Conzelmann, K. K., & Roska, B. (2013). The first stage of cardinal direction selectivity is localized to the dendrites of retinal ganglion cells. *Neuron*, **79**(6), 1078–1085.

Zhang, A.-J., & Wu, S. M. (2009). Receptive fields of retinal bipolar cells are mediated by heterogeneous synaptic circuitry. *The Journal of Neuroscience*, **29**(3), 789–797.

Additional information

Data availability statement

All relevant data are presented in the figures and the Appendix. Data are available on request from the lead author.

Competing interests

None declared.

Author contributions

M.R.E. and L.A. conceived and designed the research. L.A. performed and analysed all patch-clamp experiments. Multi-electrode array recordings and spike sorting were performed by S.R. and analysed by S.R. and L.A. L.A. prepared figures. L.A. and M.R.E. interpreted results of experiments. M.R.E., L.A. and S.R. wrote the manuscript. All authors approved the final version of the manuscript agree to be accountable for all aspects of the work in ensuring that questions related to the accuracy or integrity of any part of the work are appropriately investigated and resolved. All persons designated as authors qualify for authorship, and all those who qualify for authorship are listed.

Funding

Acknowledgements

Keywords

Supporting information

Additional supporting information can be found online in the Supporting Information section at the end of the HTML view of the article. Supporting information files available:

Peer Review History